AD-A136 721 CROSS FLOW BOILING IN TUBE BUNDLES(U) CARNEGIE-MELLON UNIV PITTSBURGH PA DEPT OF MECHANICAL ENGINEERING S C YAO OCT 83 N00014-79-C-0623 1/2

UNCLASSIFIED F/G 20/13 NL

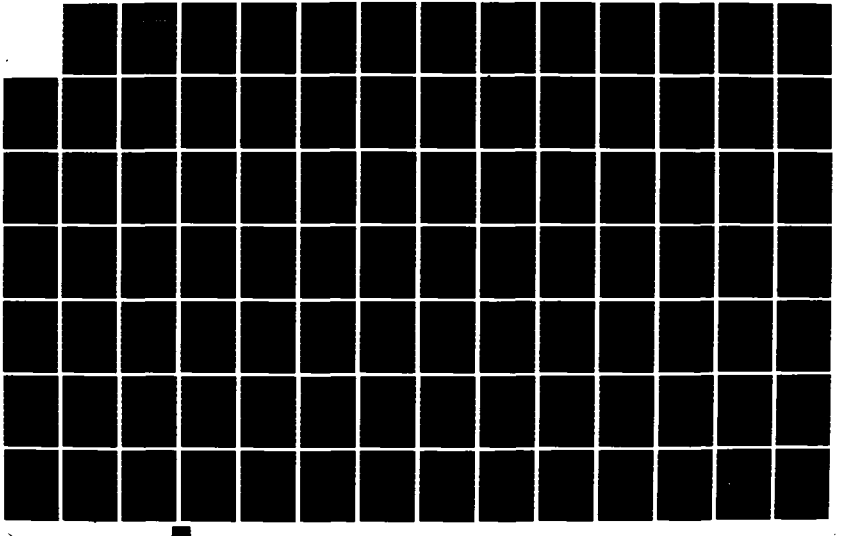

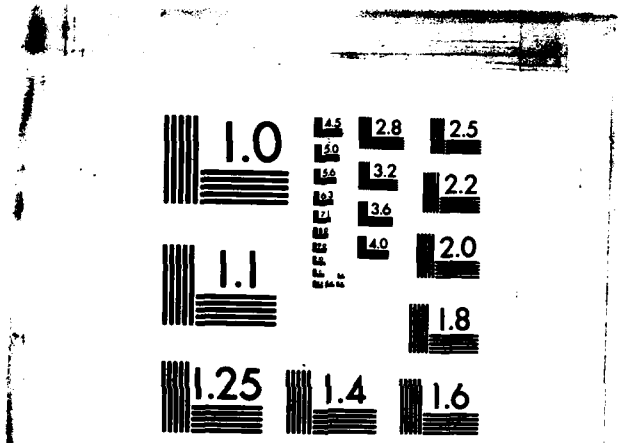

MICROCOPY RESOLUTION TEST CHART
NATIONAL BUREAU OF STANDARDS-1963-A

CMU Report N00014-79-C-0623-1-1983A

(12)

Cross Flow Boiling in Tube Bundles

Annual Technical Report
October 1983

S.C. Yao
Professor
Department of Mechanical Engineering
Carnegie-Mellon University
Pittsburgh, PA 15213

Prepared for
M.K. Ellingsworth, Program Monitor
The Office of Naval Research
Arlington, VA 22217

Under Contract No. N000014-79-C-0623, Work Unit 09-436

SECURITY CLASSIFICATION OF THIS PAGE (When Data Entered)

REPORT DOCUMENTATION PAGE

READ INSTRUCTIONS BEFORE COMPLETING FORM

1. REPORT NUMBER: N00014-79-C-0623-1983A	2. GOVT ACCESSION NO.: AD-A136721
3. RECIPIENT'S CATALOG NUMBER:	
4. TITLE (and Subtitle): CROSS FLOW BOILING IN TUBE BUNDLES	5. TYPE OF REPORT & PERIOD COVERED: Annual Technical Report Aug. 1, 1982 to Aug. 1, 1983
	6. PERFORMING ORG. REPORT NUMBER:
7. AUTHOR(s): Shi-Chune Yao	8. CONTRACT OR GRANT NUMBER(s): N00014-79-C-0623
9. PERFORMING ORGANIZATION NAME AND ADDRESS: Department of Mechanical Engineering, Carnegie-Mellon University, Pittsburgh, PA 15213	10. PROGRAM ELEMENT, PROJECT, TASK AREA & WORK UNIT NUMBERS: Program Element 6115-3N, Project RRD2403, Task Area RR0240302, Work Unit NR097-43
11. CONTROLLING OFFICE NAME AND ADDRESS: Office of Naval Research, 800 N. Quincy Street, Arlington, VA 22217	12. REPORT DATE: October 1983
	13. NUMBER OF PAGES:
14. MONITORING AGENCY NAME & ADDRESS(if different from Controlling Office):	15. SECURITY CLASS. (of this report):
	15a. DECLASSIFICATION/DOWNGRADING SCHEDULE: Unclassified

16. DISTRIBUTION STATEMENT (of this Report)

Approved for public release; distribution unlimited.

17. DISTRIBUTION STATEMENT (of the abstract entered in Block 20, if different from Report)

Same as Block No. 16.

18. SUPPLEMENTARY NOTES

19. KEY WORDS (Continue on reverse side if necessary and identify by block number)

Boiling Heat Transfer, Dryout, Corrosion, Tube Bundles

20. ABSTRACT (Continue on reverse side if necessary and identify by block number)

The research on boiling in confined spaces has been completed. This problem is of great importance to the boiling induced corrosion in the steam generator crevices between the tube and the support structures. In the report of 1981, analysis of single phase flow, two phase flow, and dryout in crevices have been presented. Experimental results of boiling and dryout in vertical crevices with closed bottom were also reported. In the report of 1982, the results of forced convective boiling heat transfer and critical heat flux in crevices are shown. In this report, the boiling heat transfer and critical heat flux in horizontal

DD FORM 1 JAN 73 1473 EDITION OF 1 NOV 65 IS OBSOLETE
S/N 0102-LF-014-6601

UNCLASSIFIED
SECURITY CLASSIFICATION OF THIS PAGE (When Data Entered)

crevices are reported.

The research on cross flow boiling in tube bundles proceeds smoothly. In this report, the analysis of single phase flow pressure drop and convective heat transfer in tube bundles at cross flow of very low or very high Reynolds numbers are presented. The experimental setup has been completed and data are taken presently.

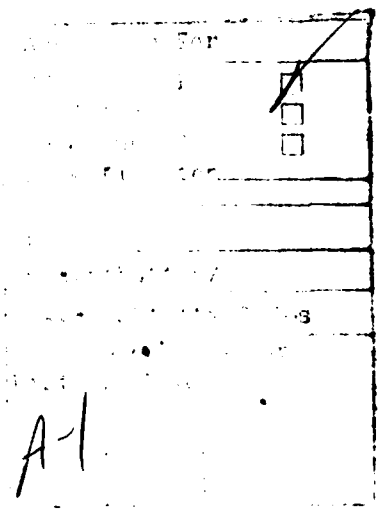

CMU Report
N00014-79-C-0623-1983A

CROSS FLOW BOILING IN TUBE BUNDLES

Annual Technical Report

October 1983

S. C. Yao
Professor
Department of Mechanical Engineering
Carnegie-Mellon University
Pittsburgh, PA 15213

Prepared for

M. K. Ellingsworth, Program Monitor
The Office of Naval Research
Arlington, VA 22217

Under Contract No. N00014-79-C-0623, Work Unit 097-436

TABLE OF CONTENTS

SUMMARY

The research on boiling in confined spaces has been completed. This problem is of great importance to the boiling induced corrosion in the steam generator crevices between the tube and the support structures. In the report of 1981, analysis of single phase flow, two phase flow, and dryout in crevices have been presented. Experimental results of boiling and dryout in vertical crevices with closed bottom were also reported. In the report of 1982, the results of forced convective boiling heat transfer and critical heat flux in crevices are shown. In this report, the boiling heat transfer and critical heat flux in horizontal crevices are reported.

The research on cross flow boiling in tube bundles proceeds smoothly. In this report, the analysis of single phase flow pressure drop and convective heat transfer in tube bundles at cross flow of very low or very high Reynolds numbers are presented. The experimental setup has been completed and data are taken presently.

CONCLUSION

Through the systematical studies of the boiling heat transfer in confined spaces the following general conclusions can be made:

(1) The boiling heat transfer in confined spaces usually has a higher heat transfer coefficient (higher heat flux at a specific wall superheat) than the conventional conditions. This is due to the effective thin film evaporation in the crevices under the squeezed pan-cake shape bubbles.

(2) The boiling regimes can be classified as isolated-deformed bubbles, coalesced-deformed bubbles, and the slightly deformed bubbles. The existence of the regimes is strongly dependent upon the Bond number of the gap as smaller, close to, or larger than unity. The Boiling number has secondary order effect to the boiling regime.

(3) The critical heat flux usually occurs at highly oscillatory conditions. The occurrence of CHF in pools can be analyzed according to flooding or momentum balance criterion. Theoretical modeling and semi-empirical correlations are established. For convective conditions, the conventional correlation can be used with a correction factor applied. The correction factor, again, depends upon the Bond number and L/D ratio of channel. The CHF decreases with decreasing gap sizes. They occur due to the dryout of the thin liquid films.

(4) With this improved understanding the designers are able to avoid the occurrence of the dryout and the induced corrosion in the crevices which are in adjacent to heated parts in boilers. A computer program has been established to predict the dryout pattern in any geometries. It can be used to examine the performance of existing equipment as well as to prove any new design concepts.

The research on cross flow heat transfer in tube bundles indicated that at low speed creeping flow the flow streams are symmetric with a cross-sectional plane; and, at very high Reynolds number single phase convection, and possibly at the convective boiling conditions the turbulence is very intense and homogeneous. Therefore the heat transfer on tubes can be described in a very simple manner that contains mainly the solidity ratio (the cross-sectional ratio of tubes to heat exchangers). As a result, the complicated Figures and Tables in presenting data of tube bundles with various configuration can be greatly simplified with short formulations. Further study is in progress to confirm this understanding on a much broader data base.

PUBLICATIONS RESULTED FROM THE PRESENT RESEARCH

1. S.C. Yao and Y. Hung, "Analysis of Fluid Flow and Heat Transfer in Heat Exchanger Tube-to-Baffle Clearances," ASME paper 81-WA/HT-10.

2. S.C. Yao and Y. Hung and J. Tang, "Analysis of Dryout in Steam Generator Crevices," ASME paper 81-WA/NE-2.

3. S.C. Yao and Y. Hung, "Heat Convection in Annular Type Crevices," Journal of Heat Transfer, Trans. ASME, Vol. 104, No. 3, pp. 403-409, 1982.

4. S.C. Yao and Y. Chang, "A Scientific Movie - Visual Study of Boiling in Narrow Gaps with Closed Bottom," presented at 7th International Heat Transfer Conference, Munich, 1982.

5. Y. Chang and S.C. Yao, "Critical Heat Flux of Vertical Narrow Annuli with Closed Bottoms," Journal of Heat Transfer, Trans., ASME, Vol. 105, No. 1, pp. 192-195, 1983.

6. S.C. Yao and Y. Chang, "Pool Boiling Heat Transfer in Confined Space," Int. Journal of Heat Mass Transfer, Vol. 26, No. 6, pp. 841-848, 1983.

7. Y.H. Hung and S.C. Yao, "Critical Heat Flux of Convective Freon-113 in Very Narrow Annuli," ASME paper 83-HT-10.

8. Y.H. Hung and S.C. Yao, "Pool Boiling Heat Transfer in Narrow Horizontal Annular Crevices," under review.

9. T.H. Hwang, and S.C. Yao, "Heat Convection and Fluid Flow in Tube Bundles at Very Low or Very High Reynolds Numbers," in preparation.

Chapter 1

Pool Boiling Heat Transfer in Narrow Horizontal Annular Crevices

ABSTRACT

Experimental results of the pool boiling in horizontal narrow annuli are reported. The effects of fluid properties, pool subcooling, crevice length, and gap size on the boiling behavior and the critical heat flux (CHF) are also studied. The CHF decreases with decreasing gap size or increasing length of the annuli. The lower CHF of narrow crevices may be explained by the thin film evaporation.

A semi-empirical correlation is established for the CHF of pool boiling in horizontal confined spaces. This correlation is compared with the CHF data of the present experiment. Satisfactory agreement is obtained.

NOMENCLATURE

Bo	Bond number for the gap, defined in equation (2)
C	A constant defined in equation (1)
CHF	Critical heat flux
d_i	Outside diameter of the heated tube [mm]
$\bar{f}$	Two-phase friction factor
Gr	Grashof number, $\beta_l \, g \, (T_w - T_s) \, d_i^3 \, / \, \nu_l^2$
g	Acceleration of gravity [m/s^2]
L	Length of the crevice [mm]
$\dot{m}_g$	Mass flow rate, defined in equation (5) [kg/s]
q	Heat flux [kw/m^2]
q_{CHF}	Critical heat flux [kw/m^2]
q_{kut}	Critical heat flux predicted by Kutateladze's correlation for a horizontal wire, defined in equation (8) [kw/m^2]
r_i	$d_i \, / \, \delta$
T_s	Ambient temperature [°C]
T_{sat}	Saturated temperature of the fluid [°C]
ΔT_{sat}	$T_w - T_{sat}$ [°C]
T_w	Wall temperature of the heated tube [°C]
v_g	Vapor velocity at the exit of the crevice [m/s]
w	Width of baffle, defined in reference [7] [mm]
y	Coordinate measured in axial direction, defined in Figure 11.

GREEK SYMBOLS

α_v	Mean void fraction, the range between 0 and 1
β_l	Thermal expansion coefficient of liquid [$^\circ C^{-1}$]
δ	Gap thickness of the crevice [mm]
λ	Latent heat of vaporization [J/kg]
μ_g	Viscosity of vapor phase [kg/ms]
μ_l	Viscosity of liquid phase [kg/ms]
ν_l	Kinematic viscosity of liquid [m^2/s]
θ_p	Angle measured from the top of the heated tube [degree]
ρ_l	Density of liquid phase [kg/m^3]
ρ_g	Density of vapor phase [kg/m^3]
σ	Surface tension of liquid phase [N/m]

INTRODUCTION

Boiling at the shell side of tube-and-shell heat exchangers, evaporators, and reboilers in the power and chemical processing devices received substantial attention in the past. Boiling may also occur in the annular crevice between the baffle plate and the heating tube. The boiling phenomena and the critical heat flux in confined vertical annuli with closed bottom have been studied by Yao and Chang [1,2]. The forced convective boiling in vertical confined annuli has been studied by Hung and Yao [3]. Presently, the boiling phenomena and the critical heat flux of confined annuli at horizontal orientation are studied in this paper with specific application to horizontal tube-and-shell heat exchangers.

Saturated pool nucleate boiling on single tubes and horizontal plates has been extensively studied. Interest has been extended to nucleate boiling heat transfer in restricted geometries. Katto and Yokoya et al. [4,5,6] investigated the nucleate pool boiling between two restricted horizontal plates. A movable artificial restriction, which is an optical assembly including an interference plate and a device for observation was placed above the heated surface. It was found that the CHF decreased with decreasing gap size. At the same heat flux, the wall temperature is invariable while the interference plate is placed comparatively apart from the heated surface (with gap size larger than 2.0 mm), but the wall temperature falls as the gap size is reduced and thereafter rises when the gap size is further reduced to very small. The dryout mechanism is suggested as a phenomenon occurred when there is an unbalance between the consumption of the liquid by evaporation on heated surface and the supply of liquid through the intermittent jetting of vapor.

Improved heat transfer characteristics with the restriction might be attributed to an

increase in the heat transfer coefficient due to vaporization from the thin liquid film on the heating surface [4,7] or increased bubble activity [8]. Jensen, Cooper, and Bergles [7] performed experiments of saturated water pool boiling at atmospheric pressure in horizontal annuli utilizing an electrically heated inner surface. Crevice heat transfer coefficients were as much as 230 % greater than those measured for conventional pool boiling. The increase in the heat transfer was explained by the thin film evaporation. The critical heat flux was found to be directly proportional to the gap size and inversely proportional to the length of annulus. However, Jensen et al. [7] did not report detailed visual observations in the narrow crevice.

As for the visual investigation of pool boiling phenomena, the existing literature is very limited. Ishibashi and Nishikawa [9] studied the saturated pool boiling heat transfer in a vertical narrow annulus with both ends open. They observed that there is a remarkable difference of heat transfer between the coalesced bubble regime and the isolated bubble regime. These regimes were separated by a critical gap size, which varied with fluid properties. The isolated bubble regime was present in larger crevices. Below the critical crevice dimension, the coalesced bubble regime was observed. Yao and Chang [1] presented a series of systematic investigations of pool boiling heat transfer in vertical narrow annuli with closed bottoms. They found that the Bond number is important in characterizing the boiling behavior in confined spaces. However, no systematic observation of pool boiling heat transfer in horizontal narrow annuli can be found in open literature.

The objectives of this paper are to establish a systematic data base of pool boiling heat transfer in narrow horizontal annuli with various working fluids and provide the explanation of the physical phenomena; and to develop a correction for the CHF prediction in horizontal annular crevices.

EXPERIMENTAL APPARATUS AND PROCEDURE

The liquid pool is established in a Pyrex tube of 101.6 mm inside diameter and 457.5 mm length with both ends closed. The liquid level is maintained by an equalizer connected to the pool, and the temperature of the pool is maintained by an immersion heater, which is adjusted by a Variac. A calibrated J-type ungrounded thermocouple is installed in the pool to measure the liquid pool temperature. The system is kept at atmospheric pressure and monitored by a pressure gauge. The generated vapor in the experiments is released and condensed before flowing back to the equalizer.

A schematic of the test section is shown in Figure 1. The heated section is a stainless steel 304 seamless tubing with 0.71 mm wall thickness, 25.4 mm O.D., and 101.6 mm heated length. Both ends of the heated tube are thermally shrink-fitted to a copper tube which has 1.42 mm wall thickness. The direct current passing through the heated tube is provided by two D.C. power supplies of different capacities. The current is measured as the voltage drop with a digital multi-meter through a calibrated shunt.

The hollow quartz cylinders are milled to an O.D. of 63.5 mm with the I.D. of 26.04, 27.00, and 30.56 mm respectively to form different gap sizes with respect to the heated tube. Both the inside and the outside surfaces of the quartz are polished to a 50-80 finish to permit visual observation of the annular crevice. Four types of annuli are formed in the present experiments. Three of them are 76.2 mm long with the gap sizes of 0.32, 0.80, and 2.58 mm respectively. The fourth annulus is 25.4 mm long with a gap size of 0.32 mm. The geometry of the concentric annulus between the heated tube and the quartz-cylinder is maintained by two spacers located at both ends of the quartz. The horizontal level of the test section is maintained during the experiment.

A pair of movable thermocouples are used to measure the inside wall temperature of the heated tube. Two J-type stainless-steel-sheathed, ungrounded thermocouples of 0.81 mm diameter are pressed against the inner-wall by plate springs with a force of 2.6 Newtons. The location of the thermocouples can be traversed axially or rotated circumferentially at the interior of the heated tube. The outer surface temperature of the tube is calculated based upon one-dimensional steady state heat conduction [10,11]. The heated surface is polished before each test with a # 320 sandpaper to ensure a consistent condition of surface finish. The calibrated thermocouples are connected to an Accurex Autodata Temperature Logger(model Ten/5) with the accuracy of $\pm 0.1^{\circ}C$.

Before each experiment the test section is preheated and preboiled for at least one hour at a low heat flux. The preheating for water test required much longer time than other fluids to remove the entrapped air bubbles. The steady state data are taken after 3 minutes for any change of heat flux.

RESULTS AND DISCUSSION

The experiments are performed with Freon-113, Acetone, and Distilled Water at atmospheric pressure. The effects of fluid properties, gap size, crevice length, and subcooling on boiling curves and critical heat flux have been investigated. Circumferential wall temperature distributions are measured. In all the experiments, the early dryout starts at the top-center point of the heated tube. This is because that at very high heat flux the top-center portion is difficult to be rewetted by incoming liquid [7,12]. Therefore, the critical heat flux in the present experiments is measured with the movable thermocouple at the top-center position of the heated tube.

In addition to these measurements, a 16 mm color movie series is edited as a record of the observations.

(A). Characteristics of the Boiling Curves

Single-phase natural convection. The natural convection around a horizontal heated circular cylinder in the range ($10^4 \leq Gr \leq 3\times10^8$) was studied by Hermann [13] and Jodlbauer [14]. They concluded that the Nusselt number is proportional to $(Gr)^{1/4}$, where Gr is based on the diameter of cylinder. That is, the heat flux q is proportional to $(T_w - T_s)^{5/4}$. Therefore, the relationship becomes

$$q = C (T_w - T_{sat})^{5/4} \quad (1)$$

The experimental data of single-phase natural convection of a single tube with Freon-113 is shown in Figure 2. The C value in equation (1) is found to be 0.125 for Freon-113.

The temperature distributions of Freon-113 at various measuring locations with gap size of 0.32 mm and crevice length of 76.2 mm are shown in Figure 3.

The location where y/L equals zero represents the edge of the crevice. At the same gap size and θ_p (the location of $\theta_p = 0$ is at the top of heated tube), the temperature is increased with the increasing y/L, that means the single-phase heat transfer is the worst at the center plane of the heated crevice. The temperature at the bottom of heated tube is lower than that at the top of heated tube. Similar results are observed for acetone and distilled water. It is observed that the trend of temperature distribution is almost the same for various gap sizes. However, the smaller the gap size, the higher the wall temperature for a same heat flux.

Boiling Inception. When heat flux is increased an overshoot of the wall superheat beyond saturation happens before the inception of the boiling. In the present

experiment an interesting phenomenon which should be pointed out is the stability of the boiling inception. Two different kinds of boiling inception are observed : the local boiling inception which occurs at the top of the heated tube, and the overall boiling inception which occurs simultaneously over the whole tube. Without observation, if the temperature measuring position is at the bottom of the heated tube, the local boiling inception at the top of the tube can not be detected easily.

For the tests of Freon-113 and acetone with 2.58 mm gap size and open tube (i.e. single tube without confinements), the local boiling inception occurs first, then the overall boiling inception happens at a higher heat flux. For the tests using distilled water the phenomenon of local boiling inception is usually not observed. The existence of local boiling inception in horizontal annular crevices could be related to their Bond number, which relates the gap size and the capillary constant.

$$Bo = \frac{\delta}{[\sigma/g(\rho_l-\rho_g)]^{1/2}} \qquad (2)$$

The range of Bond number in the present experiments is listed in Table 1.

Before the boiling inception, the top portion of the heated tube where the temperature is comparatively high will be more likely to initiate the boiling.

For the case of Bo≥1.0, after the boiling inception the bubbles are close to the spherical shape and they flow away easily. When the heat flux is gradually increased, the bubbles may also initiate at the bottom portion of the tube that the overall boiling inception occurs.

For the cases of Bo < 1.0, the generated bubbles are usually deformed in the gap. This phenomenon is also observed in [1]. During the boiling inception the bubbles expand into the form of isolated-deformed bubbles and propagate in the gap. Then

they coalesce over the whole heated surface. Therefore, only the overall boiling inception is observed.

Nucleate pool boiling. The nucleate boiling curves of the experiments are shown in Figures 4, 5, and 6. At a same heat flux, the wall temperature is decreased with reducing gap sizes except for the cases of acetone and distilled water with the smallest gap of 0.32 mm.

The increased heat transfer within the narrow crevices might be attributed to the increased bubble activity [8] and the vaporization of the thin film on the heated surface [7,9]. In confined spaces, at a fixed heat flux, the masses of vapor generated is constant so that with decreasing gap size higher vapor velocities are induced. With the increased vapor velocities, the shear stress on the liquid film at the heated surface increases and the liquid film is reduced in thickness. Since the major heat transfer resistance is the heat conduction across the liquid film, the reduced film thickness increases the heat transfer coefficient.

In the present experiments of acetone and distilled water with gap size of 0.32 mm and high heat flux, the wall temperature is higher than that in the cases of gap sizes of 0.80 and 2.38 mm as shown in Figures 5 and 6. This is because the intermittency of partial dryout and rewetting due to fluid oscillation leads to a wall temperature oscillation (the shaded area in Figures) and a higher wall temperature. Similar phenomenon has been observed by Katto et. al [4], Jensen et. al [7], and Yao et. al [1].

Critical heat flux. At high heat fluxes, because of the space restriction, numerous coalesced vapor bubbles occur, grow, and rapidly spread over the heated surface. The area of heated surface is wet by a thin liquid film while the vaporization takes place. During the growth period of the bubble, liquid can not be supplied to the heated

surface. The bubble grows continuously until one of the following two situations occurs : the liquid film underneath the expanding bubble evaporates completely and thereby terminates the driving force for growth, or the bubble grows to such a size that it extends beyond the edge of the restriction. Then the buoyancy makes the bubble to flow out of the crevice, and the liquid flows into the crevice and rewets the surface. After rewetting, the same cycle starts again. As the heat flux is increased, dry spots begin to appear at the end of the cycle. If liquid does not rewet the surface within a certain time, the temperature of the dried portion may become high enough to initiate dryout earlier in the next cycle. Therefore, the CHF occurs. With the fluid circulation retarded when the gap is reduced, rewetting of the heated surface will be more difficult and the CHF becomes lower. The present CHF data at saturated condition are listed in Table 1.

(B). Effect of Measuring Location

Typical boiling curves measured at the top and the bottom positions of the heated tube are compared in Figure 7. This is the case when Bond number is less than unity that the overall boiling occurs in the gap at the boiling inception. Before the boiling inception the heat transfer at the bottom of heated tube is higher. At the overall boiling inception, the temperature decrease at the top is more than that at the bottom. After the boiling inception, the heat transfer at the top portion is dominated by thin film evaporation, and the heat transfer coefficient is therefore higher than that at the bottom. As heat flux is further increased, the thin liquid film underneath the squeezed bubbles may dry up easily. Finally, the permanent dryout at the top may occur and an early CHF is reached.

(C). Effect of Crevice Length

In the experiments of Freon-113 with gap size of 0.32 mm, as the length of crevice is decreased from 76.2 mm to 25.4 mm, the overall boiling curve is changed as shown in Figure 8. The single-phase natural convective heat transfer of long crevice is lower than that of the short crevice due to the higher resistance of the flow. After the boiling inception, the local nucleate boiling heat transfer at the top-center of long crevice length is higher mainly because the heat transfer at the top is dominated by thin film evaporation. At higher heat flux, it is difficult to rewet the top-center portion of the long crevice, then the CHF of the longer crevice occurs at a lower heat flux.

(D). Effect of Pool Subcooling

In the subcooled tests, the pool temperature is kept at 25°C subcooling with the crevice gap size of 0.32 mm. The boiling curve of subcooled condition is compared with that of saturated condition in Figure 9. As expected, the subcooling enhances the boiling heat transfer.

(E). Boiling Curve of the Line-Contact Configuration

Figure 10 shows the boiling curve for the configuration of line-contact of the heated tube and the quartz shroud at the top of the eccentric crevice. When heat flux is increased to 6.05 kw/m^2, a permanent dryout zone is observed at the top contacted location. According to the experimental results by Baum and Curlee [15], the occurrence of permanent dryout in some steam generators may lead to local chemical concentration build-up, and the consequent corrosion. As shown in the Figure 10 the

maximum heat flux, which does not lead to permanent dryout when a line-contact occurs, is much less than the CHF of the corresponding situation with concentric configuration of the annulus.

(F). Semi-empirical CHF Correlation

A correlation has been developed by Jensen et al. [7] relating the critical heat flux to the geometry of the horizontal tube-baffle crevice and fluid properties. Using a least-square fit, the following empirical equation was obtained :

$$\left[\frac{q_{CHF} L r_i^2}{4\lambda \mu_g (r_i+1)} \right] \left[\frac{\rho_l - \rho_g}{\rho_g} \right]^{0.78} = 2.994\times10^5 \left[\frac{\delta}{L} \right]^{-0.213} \quad (3)$$

The comparison of the equation (3) with the present CHF data is shown in Table 1. The prediction of equation (3) shows satisfactory agreement with the present data for the small gap of 0.32 mm and the short crevice length of 25.4 mm, but this equation is not adequate for the long crevices. This is because the test conditions in [7] correspond to the cases of the small gap size and short crevice length in the present experiments. In order to predict the CHF in a wide range of the present data, a semi-empirical modelling is established.

The schematic of the test section is shown in Figure 11-a. Due to the symmetry, the analysis has only to apply for a quarter portion of the whole annulus. The flow channel for the present analysis is shown in Figure 11-b. The gap size is generally assumed much smaller than the radius of heated tube such that the curvature of the crevice can be neglected. The flow channel of the crevice is split into two flattened regions as shown schematically in Figure 11-b with the additional assumptions :

1. The flow is driven by the buoyancy in the Region I, and balanced by the viscous drag force in the Region II.

2. The fluid quality at the bottom of the annulus is zero. When the critical heat flux occurs the fluid quality at the upper exit of the annulus is unity.

3. The overall width of the channel where the vapor flows out at the top portion of the annulus (Region II) is $d_i/2$.

Following the assumptions (1) and (2), the balance of the buoyant driving force and the frictional force can be expressed as

$$\alpha_v (\rho_l - \rho_g) g d_i = \bar{f} \left[\frac{L/2}{2\delta} \right] \left[\frac{\rho_g v_g^2}{2} \right] \quad (4)$$

where α_v is the mean void fraction in Region I. In this analysis, we assume $\alpha_v = 1/2$.

The mass flow rate of the vapor at the exit is

$$\dot{m}_g = \rho_g v_g \left(\frac{d_i}{4} \right) \delta \quad (5)$$

The critical heat flux can be obtained from the conservation of energy, that is

$$\dot{m}_g \lambda = q_{CHF} \left(\frac{L}{2} \right) \left(\frac{\pi d_i}{2} \right) \quad (6)$$

Combining Equations (4), (5), and (6), the predicted CHF q_{CHF} becomes

$$q_{CHF} = F(\bar{f}) \left[Bo^{1/2} \left(\frac{\delta}{L} \right) \left(\frac{d_i}{L} \right)^{1/2} \right] q_{kut} \quad (7)$$

where q_{kut} is the critical heat flux predicted by Kutateladze's correlation for a horizontal wire in liquid pool [16].

$$q_{kut} = K^{1/2} \lambda \rho_g^{1/2} [\sigma g (\rho_l - \rho_g)]^{1/4} \quad (8)$$

with the average value of $K^{1/2}$ set at 0.14.

The $F(\bar{f})$ is a function of the two-phase friction factor. The two-phase friction

factor $\bar{f}$ is dependent upon μ_l and μ_g [17], and it should be also affected by Bond number for narrow annuli. Therefore, the function F can be expressed generally in the following non-dimensional form

$$F(\bar{f}) = F\left(\frac{\mu_g}{\mu_l}, Bo\right) \tag{9}$$

The semi-empirical function F can be determined from the best fit to the present data of experiments. That gives

$$F\left(\frac{\mu_g}{\mu_l}, Bo\right) = 110 \left(\frac{\mu_g}{\mu_l}\right)^{0.3} \exp\left(-0.65Bo\right) \tag{10}$$

Finally, the present semi-empirical correlation is obtained from equations (7), (8), and (10).

The experimental data and the prediction of this semi-empirical formulation have been compared in Table 1. The average error is 18 % with the maximum error less than 28 %. In the present study, the maximum effect of the (μ_g/μ_l) term in the correlation for various working fluids is 26 %.

CONCLUSIONS

Based on the present study, the following conclusions may be drawn :

1. Two types of boiling inception are observed, i.e. local boiling inception and overall boiling inception. This phenomenon can be related to the Bond number. Generally, no local boiling inception is observed when the Bond number is less than unity.

2. After the overall boiling inception, the boiling heat transfer at the top portion of the heated tube is possibly dominated by thin film evaporation. During all the experiments, the early critical heat flux occurs at the top-center point of the heated tube.

3. Sustained flow oscillation is observed in the tests of 0.32 mm gap size. Occasionally, the wall temperature of this narrow crevices at nucleate boiling is higher than that of larger gaps. This is due to the intermittency of partial dryout and rewetting which leads to an obvious temperature oscillation and the higher wall temperature in narrow crevices.

4. Boiling phenomena of an eccentric annulus with the configuration of line-contact at the top of heated tube are investigated. A permanent dryout zone occurs at the top portion of the heated tube at low heat flux.

5. The CHF decreases with decreasing gap size or increasing length of the annuli. The mechanism of CHF in confined spaces is related with the dryout of the thin liquid film on the heated surface.

6. A model for the critical heat flux has been developed, and a semi-empirical correlation has been established. The comparison between this correlation and the present CHF data has been made with satisfactory agreement.

REFERENCES

1. Yao, S. C. and Chang, Y.,"Pool Boiling Heat Transfer in Confined Spaces," *Int. J. Heat Mass Transfer*, Vol.26, No.6, 1983, pp.841-848.

2. Yao, S. C. and Chang, Y.,"Critical Heat Flux of Vertical Narrow Annuli with Closed Bottoms," Trans. ASME, *J. of Heat Transfer*, Vol.105, 1983, pp.192-195.

3. Hung, Y. H. and Yao, S. C.,"Critical Heat Flux of Convective Freon-113 in Very Narrow Annuli." 83-HT-10, ASME 21st National Heat Transfer Conference, Seattle, Washington, July 24-28, 1983.

4. Katto, Y. and Yokoya, S.,"Experimental Study of Nucleate Pool Boiling in Case of Making Interference-Plate Approach to the Heating Surface," Third International Heat Transfer Conference, 1966, pp.219-227.

5. Katto, Y. and Yokoya, S.,"Principle Mechanism of Boiling Crisis in Pool Boiling," *Int. J. Heat Mass Transfer*, Vol.11, 1968, pp.993-1002.

6. Katto, Y., Yokoya, S., and Ysunaka, M.,"Mechanism of Boiling Crisis and Transition Boiling in Pool Boiling," Proceedings of the Fourth Int. Heat Transfer Conference, Vol.5, B3.2, 1970.

7. Jensen, M. K., Cooper, P. E., and Bergles, A. E.,"Boiling Heat Transfer and Dryout in Restricted Annular Geometries," 16th National Heat Transfer Conference, *AICHE*, Paper No. AICHE-14, 1976, pp.205-213.

8. Plevyak, T. J.,"Improved Boiling Heat Transfer with Induced Vapor Bubble Mixing," ASME paper No. 68-WA/HT-29, 1968.

9. Ishibashi, E. and Nishikawa, K.,"Saturated Boiling Heat Transfer in Narrow Space," *Int. J. Heat Mass Transfer*, Vol.12, 1969, pp.863-894.

10. Lung, H., Latsch, K., and Rampf, H.,"Boiling Heat Transfer to Subcooled Water in Turbulent Annular Flow," CHapter 10, *Heat Transfer in Boiling*, Hemisphere Publishing Corporation, Washington, 1977, pp.219-235.

11. Hennecke, D. K. and Sparrow, E. M.,"Local Heat Sink on A Convectively Cooled Surface-Application to Temperature Measurement Error," *Int. J. Heat Mass Transfer*, Vol.13, 1970, pp.287-304.

12. Costello, C. P. and Frea, W. J.,"A Salient Nonhydrodynamic Effect on Pool Boiling Burnout of Small Semicyclindrical Heaters." Chemical Engineering Progress Symposium Series, Vol.61, No.57, 1965, pp.258-268.

13. Hermann, R.,"Wärmeübertragung bei freier Strömung am waagerechten Zylinder in zweiatomigen Gasen," VDI-Forschungsheft, 1936, p.379.

14. Jodlbauer, K.,"Das Temperatur- und Geschwindigkeitsfeld um ein geheiztes Rohr bei freier Konvektion. Forschg. Ing.-Wes. 4, 1933, pp.157-172.

15. Baum, A. J. and Curlee, N. J., Jr., "An Experimental and Analytical Investigation of Dryout and Chemical Concentration in Confined Geometries," ASME Nuclear Eng. Division Conference, San Francisco, August 18-21, 1980.

16. Kutateladze, S. S.,"Heat Transfer in Condensation and Boiling," USAEC Report AEC-tr-3770, 1952.

17. Collier, J. G., *Convective Boiling and Condensation*, McGraw-Hill, London, 1972, pp.28-32.

LIST OF TABLES

LIST OF FIGURES

Table 1 : The Range of Bond Number and the CHF Data in the Present Experiments

Tube	O.D. : 25.4 mm
	Thickness : 0.71 mm
	Material : Stainless Steel 304 Seamless Tubing
Operating Pressure	1 atm
Pool Temperature	25°C Subcooling - Saturation

Woring Fluid	L (mm)	δ (mm)	Bo	Exp. q_{CHF} (kw/m^2)	Pred. q_{CHF} (kw/m^2) [I]	Pred. q_{CHF} (kw/m^2) [II]	% Error of [II]
Freon-113	76.2	0.32	0.30	12.2	17.5	8.8	-27.8
Freon-113	76.2	0.80	0.74	27.8	36.6	26.1	- 6.3
Freon-113	76.2	2.58	2.38	63.7	98.2	51.9	-18.6
Freon-113	25.4	0.32	0.30	35.7	41.5	45.7	28.4
Acetone	76.2	0.32	0.20	16.1	30.8	14.3	-11.3
Acetone	76.2	0.80	0.50	55.0	64.6	46.5	-15.4
Acetone	76.2	2.58	1.60	110.5	173.3	131.7	19.2
Acetone	25.4	0.32	0.30	94.7	73.2	74.2	-21.6
Distilled Water	76.2	0.32	0.13	33.9	58.4	41.1	21.4

[I] : CHF predicted by the equation (3), Ref. [7].

[II] : CHF predicted by equations of (7),(8),and (10).

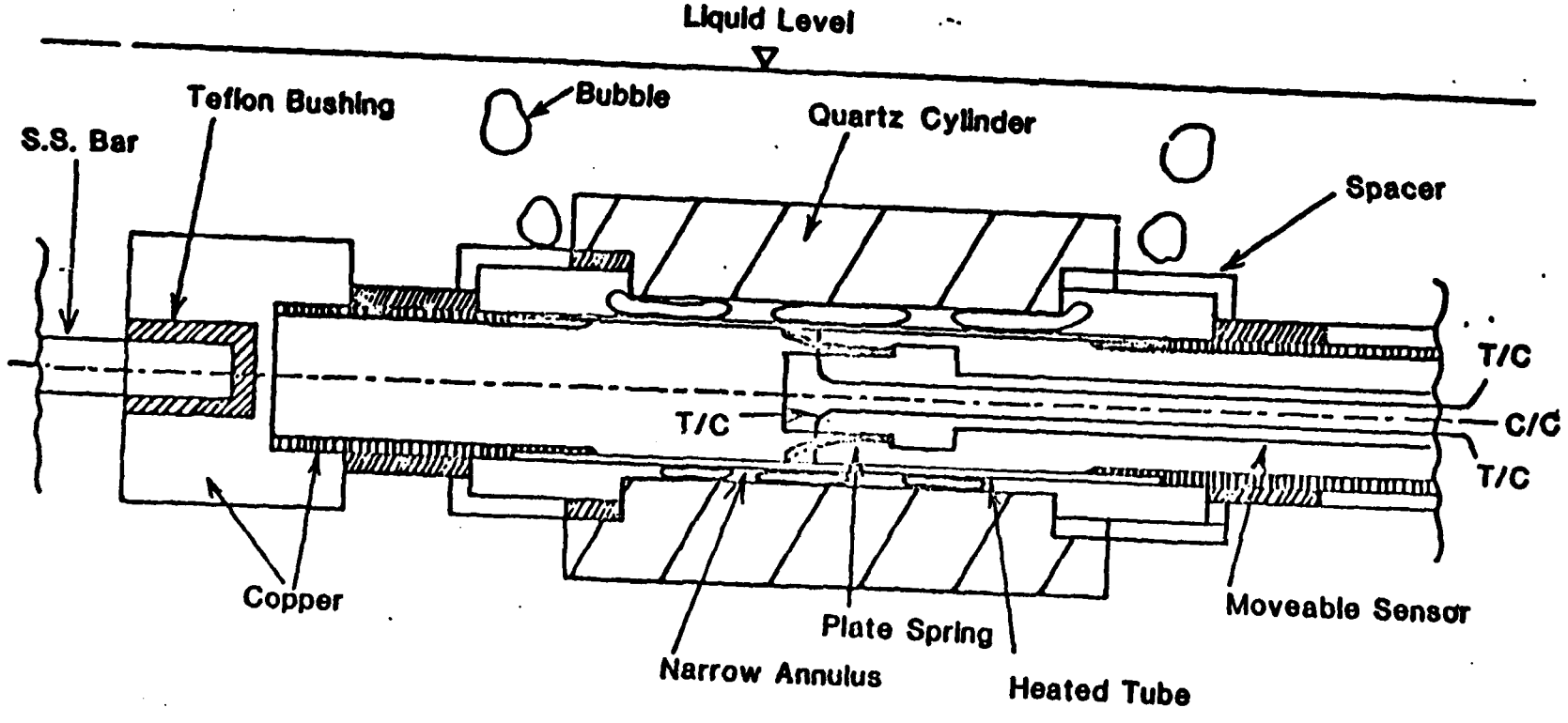
Liquid Level
Teflon Bushing
Bubble
S.S. Bar
Quartz Cylinder
Spacer
T/C
T/C
C/C
T/C
Copper
Narrow Annulus
Plate Spring
Heated Tube
Moveable Sensor

Fig. 1

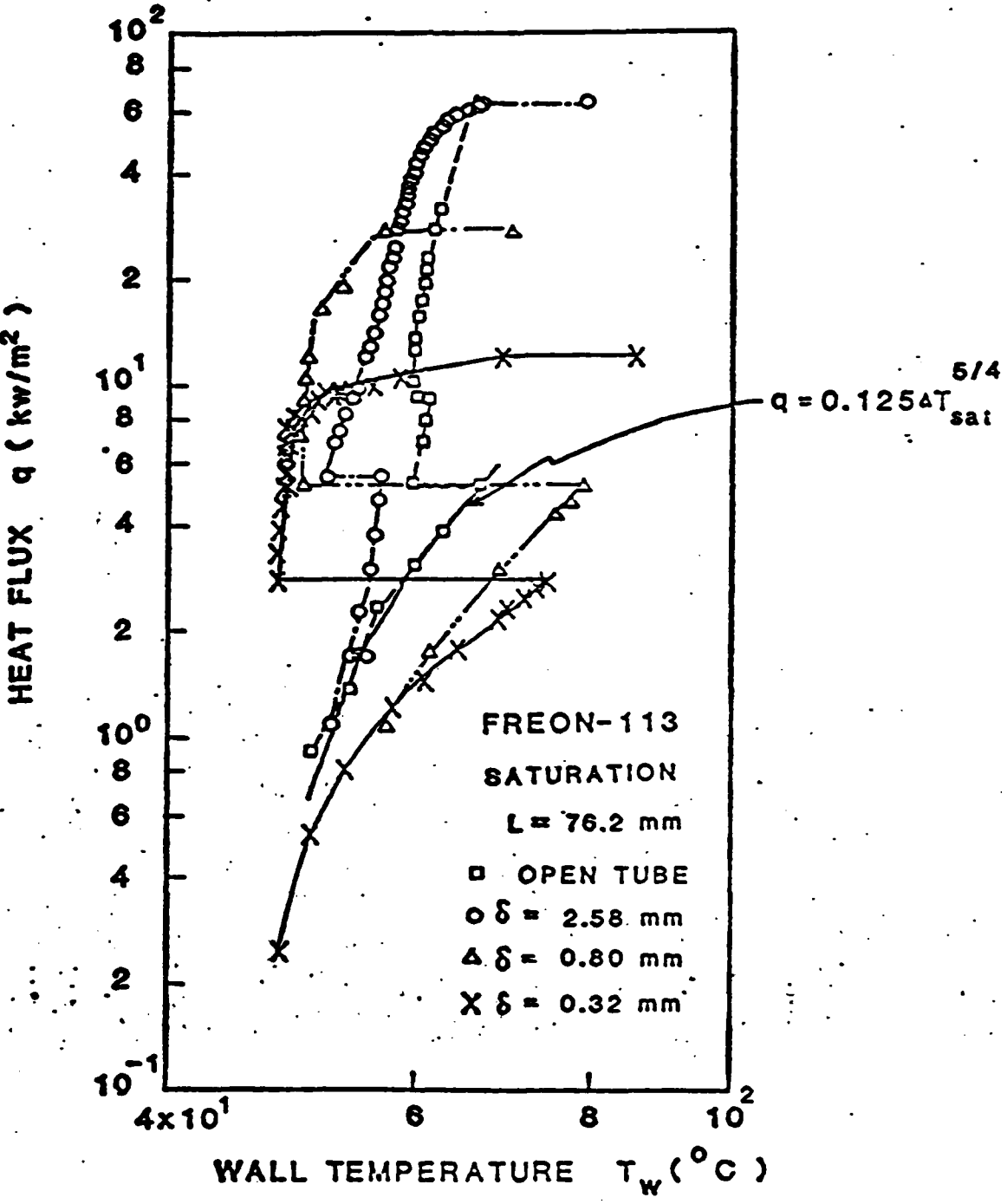
HEAT FLUX q (kw/m²)
WALL TEMPERATURE T_w (°C)
$q = 0.125 \Delta T_{sat}^{5/4}$
FREON-113
SATURATION
L = 76.2 mm
□ OPEN TUBE
○ δ = 2.58 mm
△ δ = 0.80 mm
× δ = 0.32 mm

Fig. 2

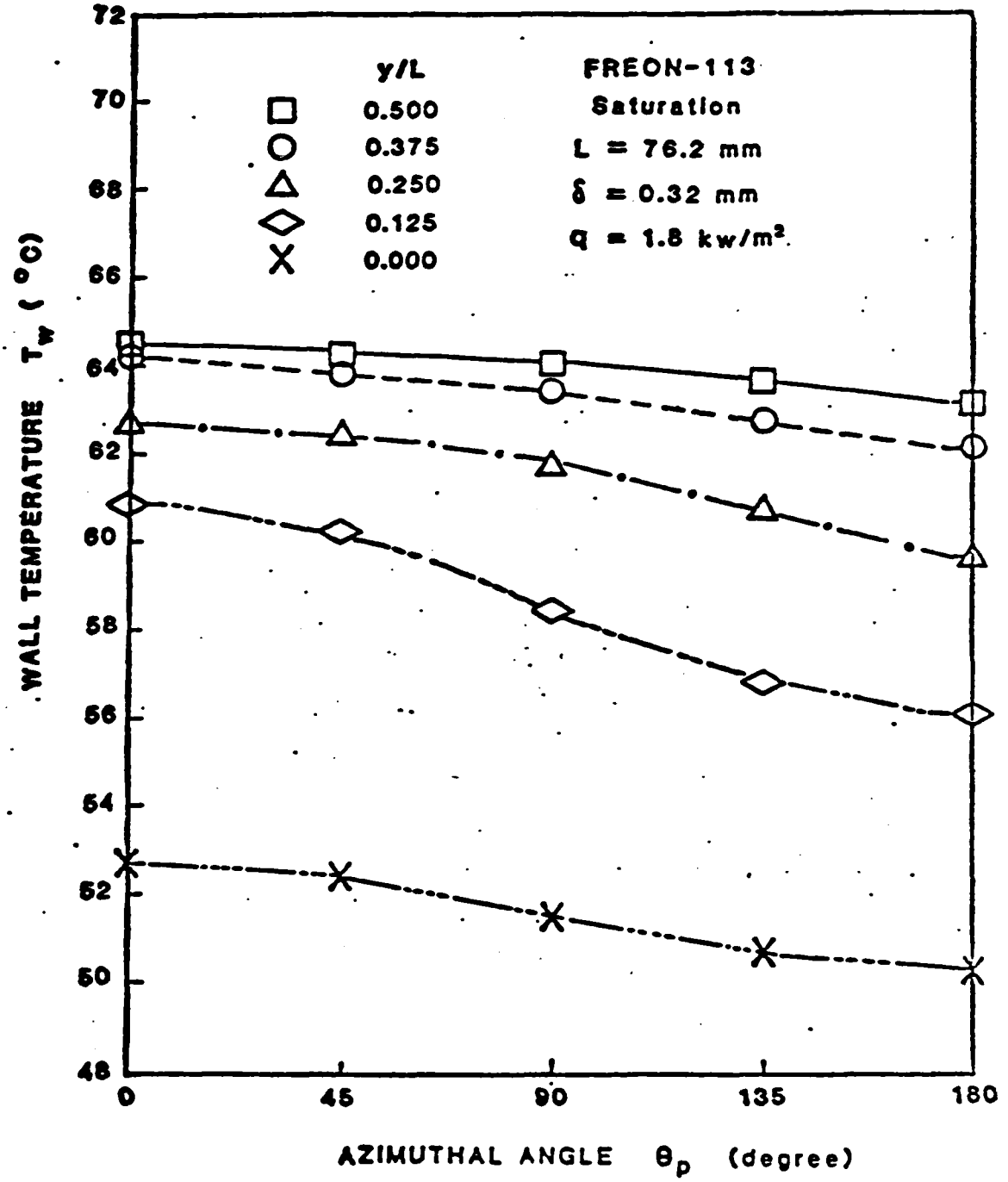
y/L
0.500
0.375
0.250
0.125
0.000
FREON-113
Saturation
L = 76.2 mm
δ = 0.32 mm
q = 1.8 kw/m²
WALL TEMPERATURE T_w (°C)
72
70
68
66
64
62
60
58
56
54
52
50
48
0
45
90
135
180
AZIMUTHAL ANGLE θ_p (degree)

Fig. 3

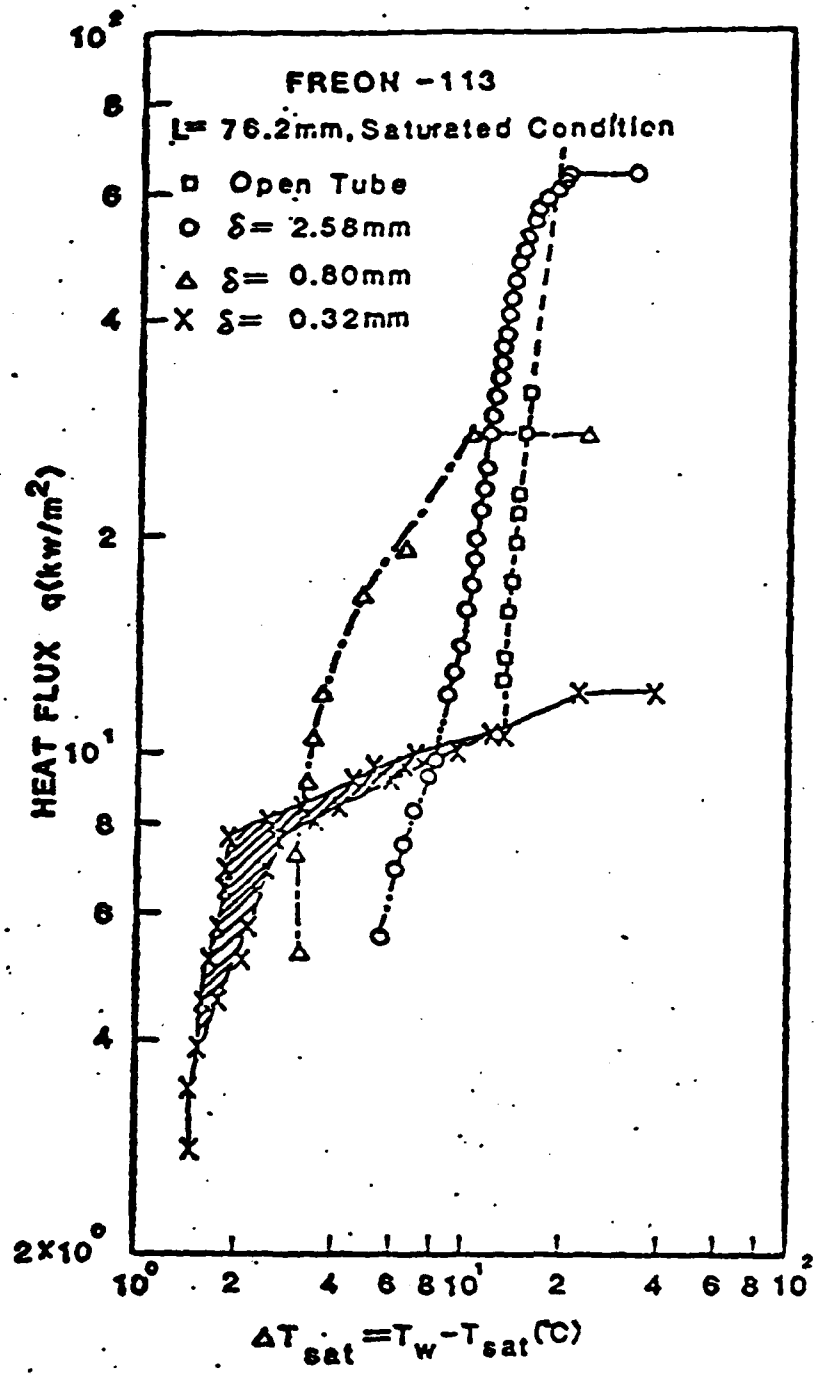
FREON -113
L= 76.2mm, Saturated Condition
Open Tube
δ= 2.58mm
δ= 0.80mm
δ= 0.32mm
HEAT FLUX q(kw/m²)
ΔT_sat = T_w - T_sat (°C)

Fig. 4

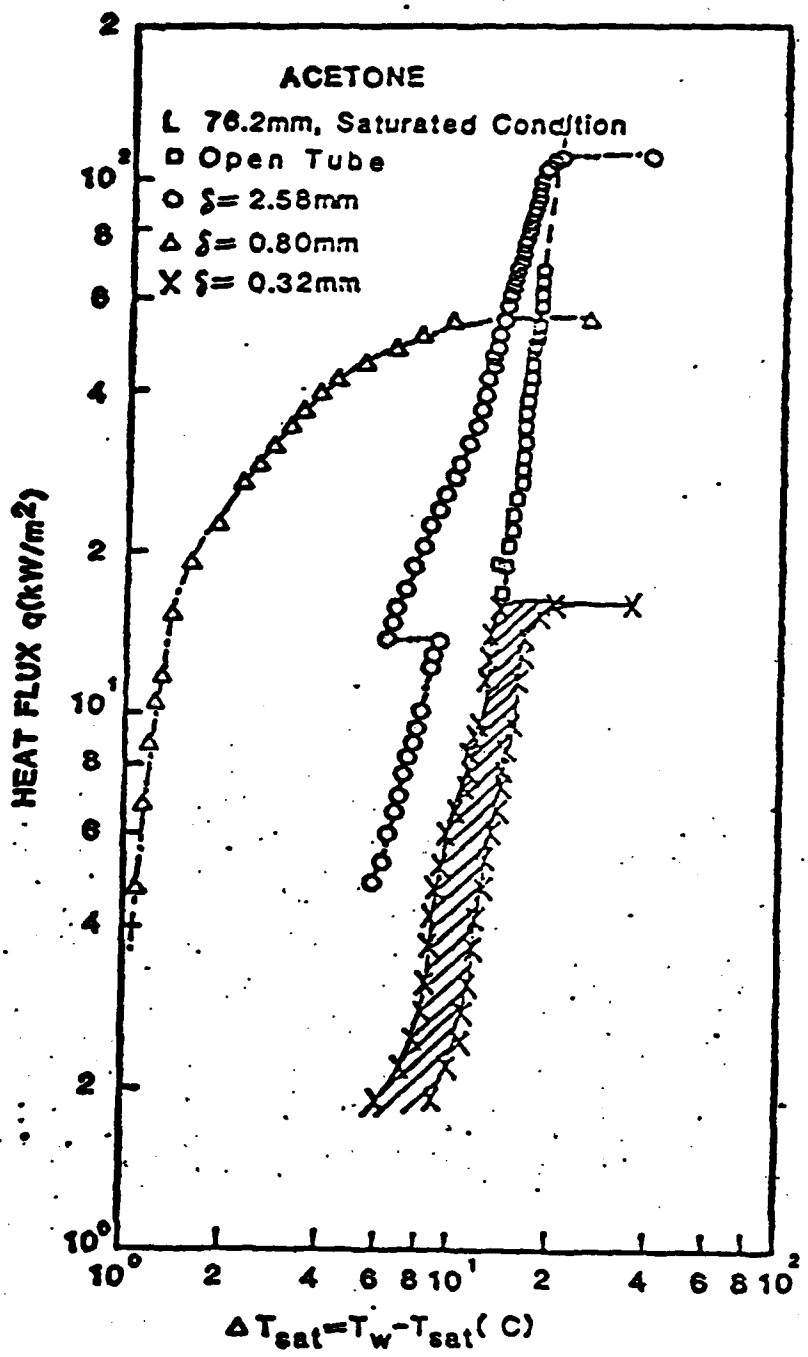
ACETONE
L 76.2mm, Saturated Condition
□ Open Tube
○ δ= 2.58mm
△ δ= 0.80mm
X δ= 0.32mm
HEAT FLUX q(kW/m²)
ΔTsat=Tw-Tsat(C)

Fig. 5

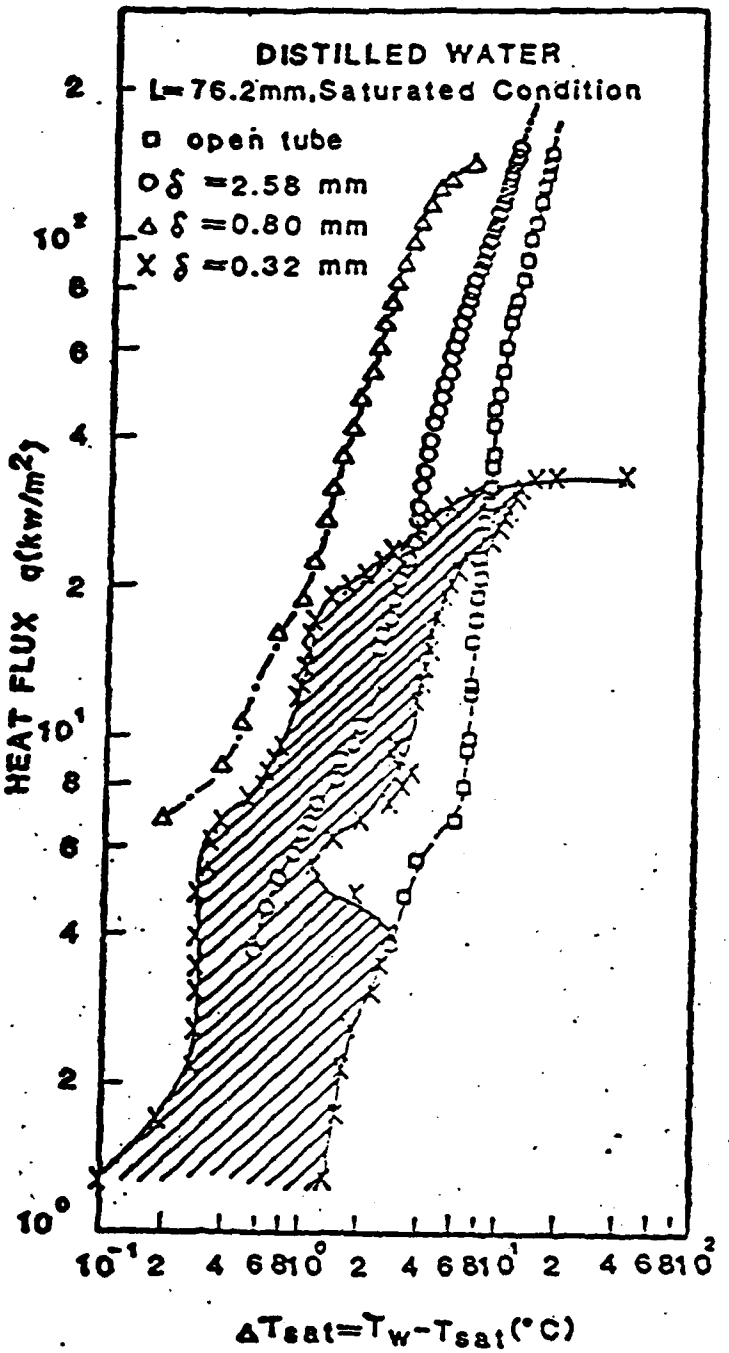
DISTILLED WATER
L=76.2mm, Saturated Condition
□ open tube
○ δ =2.58 mm
△ δ =0.80 mm
X δ =0.32 mm
HEAT FLUX q(kw/m²)
ΔTsat=Tw-Tsat(°C)

Fig. 6

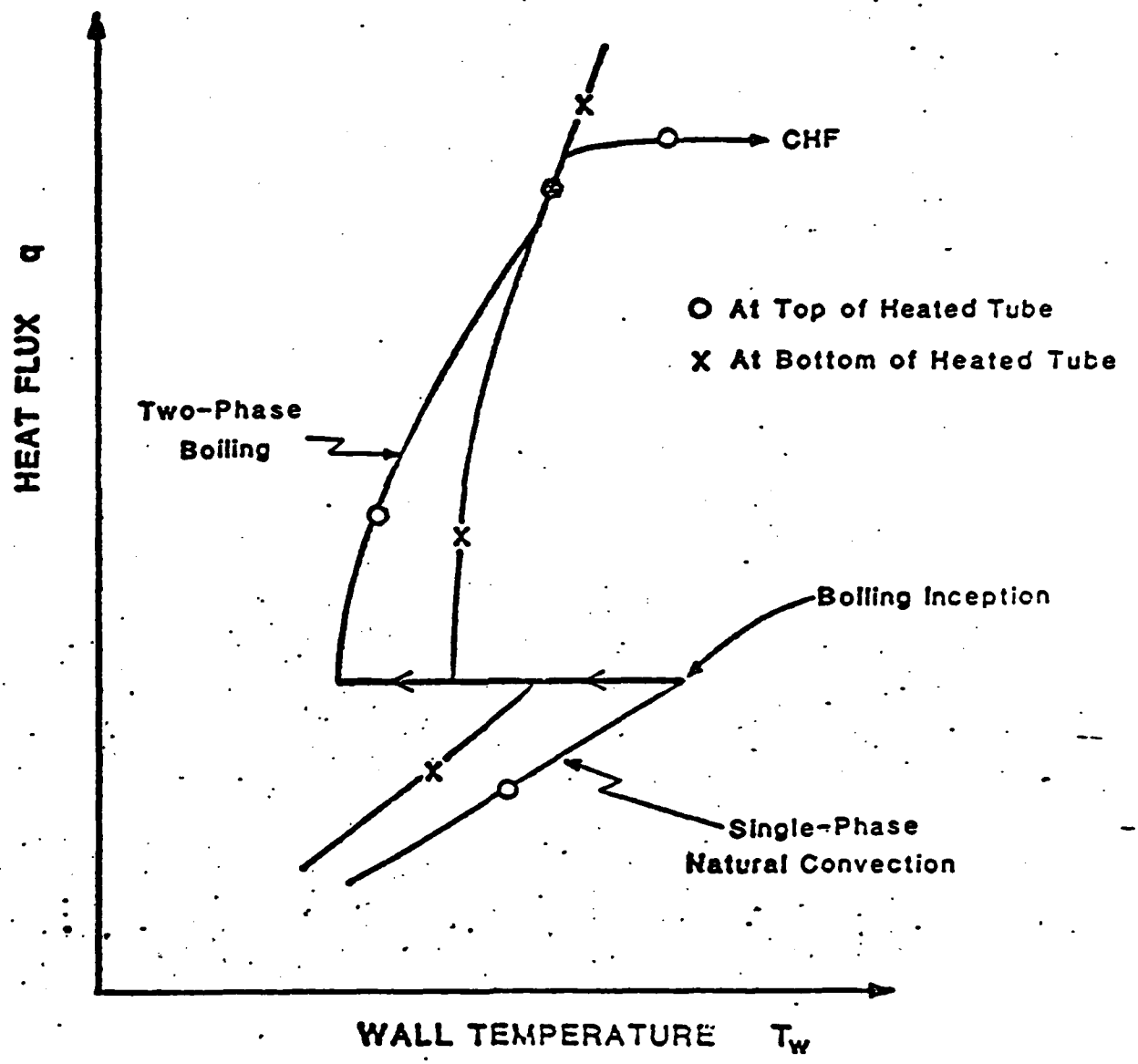
HEAT FLUX q
CHF
O At Top of Heated Tube
X At Bottom of Heated Tube
Two-Phase
Boiling
Boiling Inception
Single-Phase
Natural Convection
WALL TEMPERATURE T_w

Fig 7

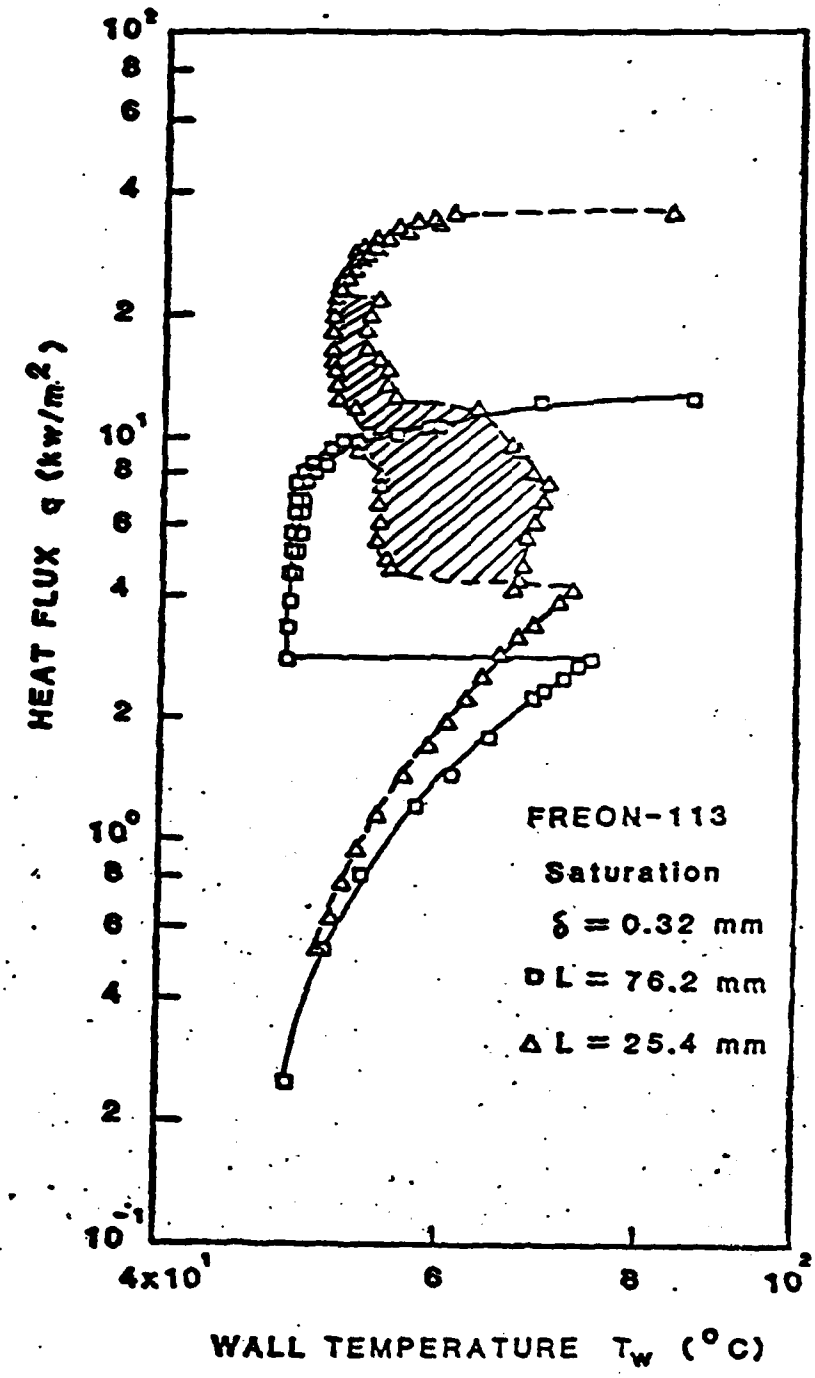
HEAT FLUX q (kw/m²)
WALL TEMPERATURE T_w (°C)
FREON-113
Saturation
δ = 0.32 mm
□ L = 76.2 mm
△ L = 25.4 mm

Fig. 8

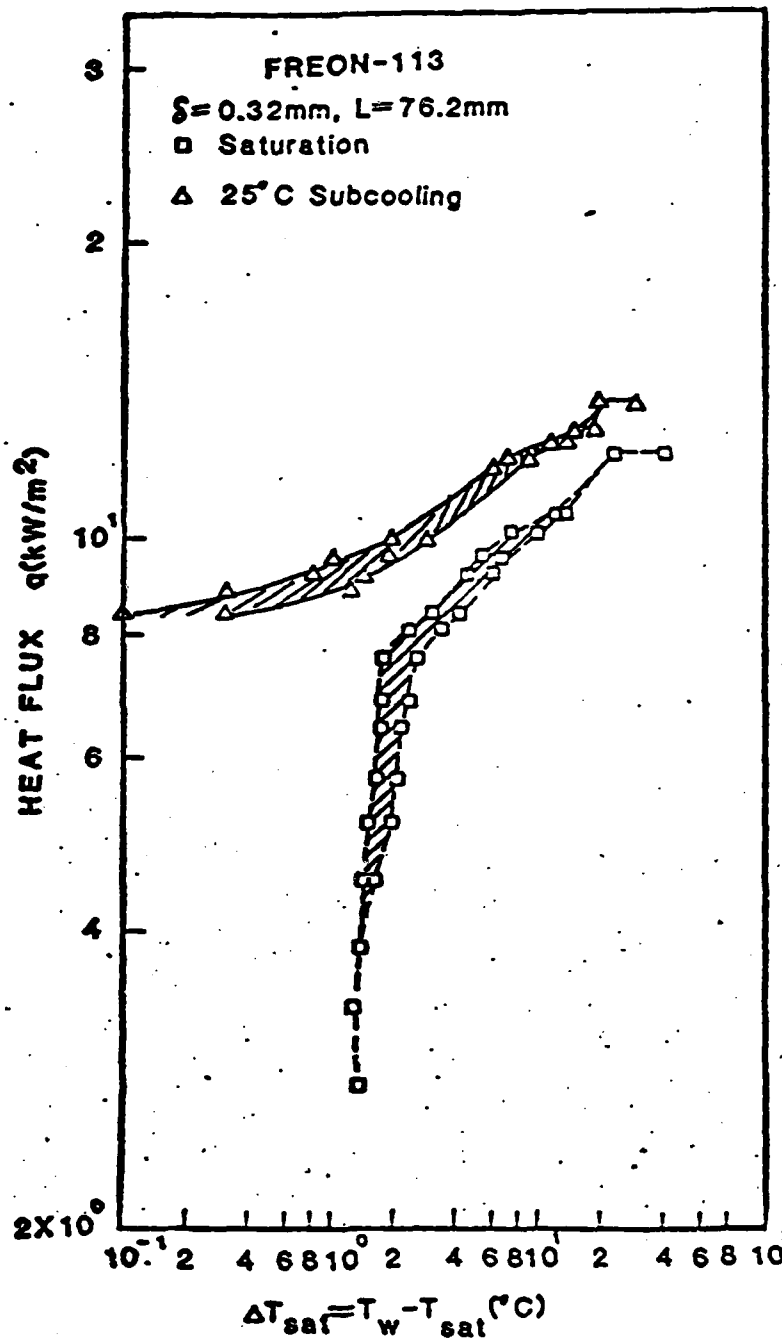
FREON-113
δ= 0.32mm, L=76.2mm
Saturation
25°C Subcooling
HEAT FLUX q(kW/m²)
3
2
10¹
8
6
4
2X10⁰
10⁻¹ 2 4 6 8 10⁰ 2 4 6 8 10¹ 2 4 6 8 10²
ΔT_sat=T_w-T_sat(°C)

Fig. 9

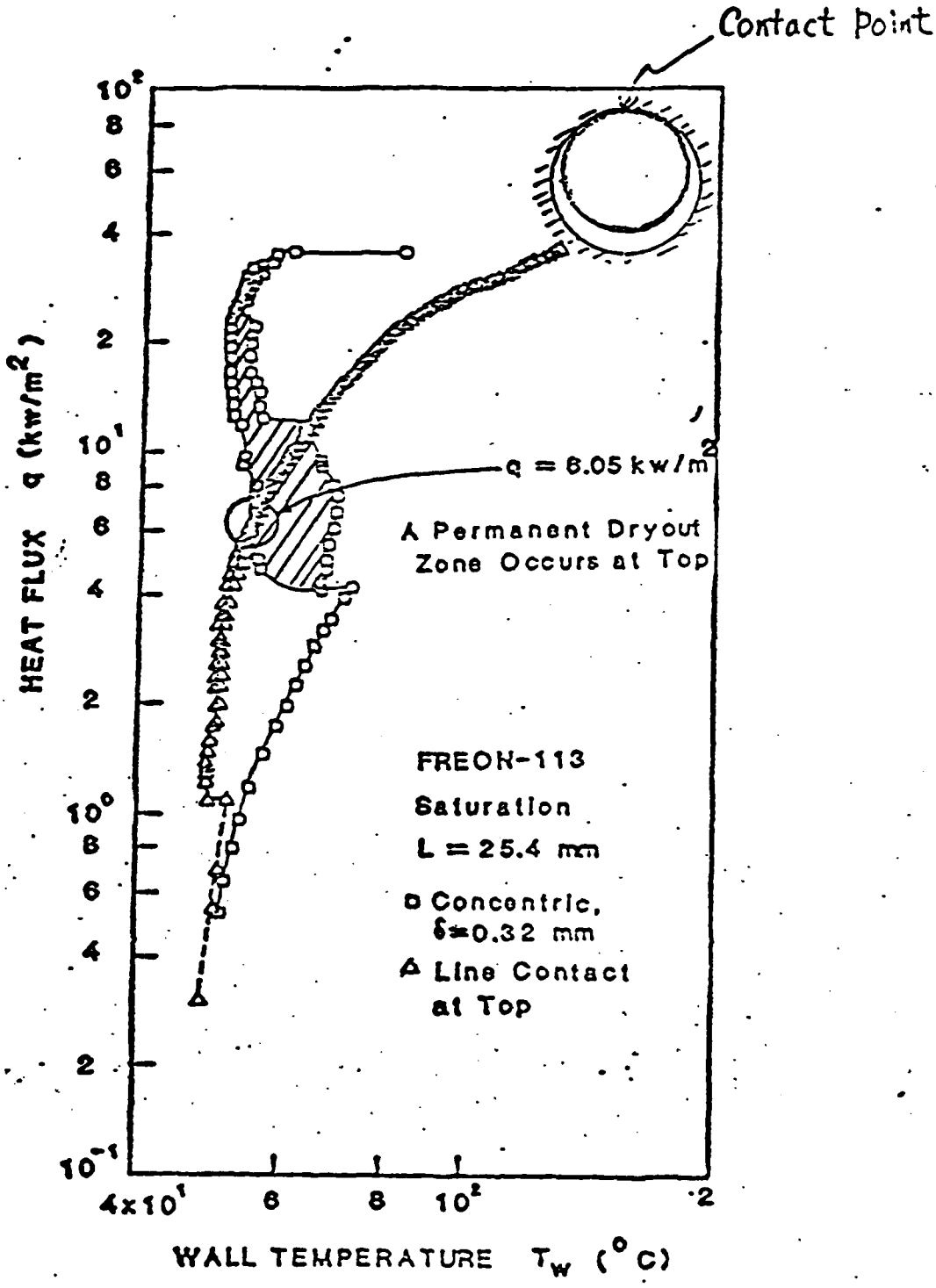
Contact Point
HEAT FLUX q (kw/m²)
10²
8
6
4
2
10¹
8
6
4
2
10⁰
8
6
4
2
10⁻¹
q = 6.05 kw/m²
A Permanent Dryout Zone Occurs at Top
FREON-113
Saturation
L = 25.4 mm
□ Concentric, δ=0.32 mm
△ Line Contact at Top
4x10¹
6
8
10²
2
WALL TEMPERATURE Tw (°C)

Fig 10

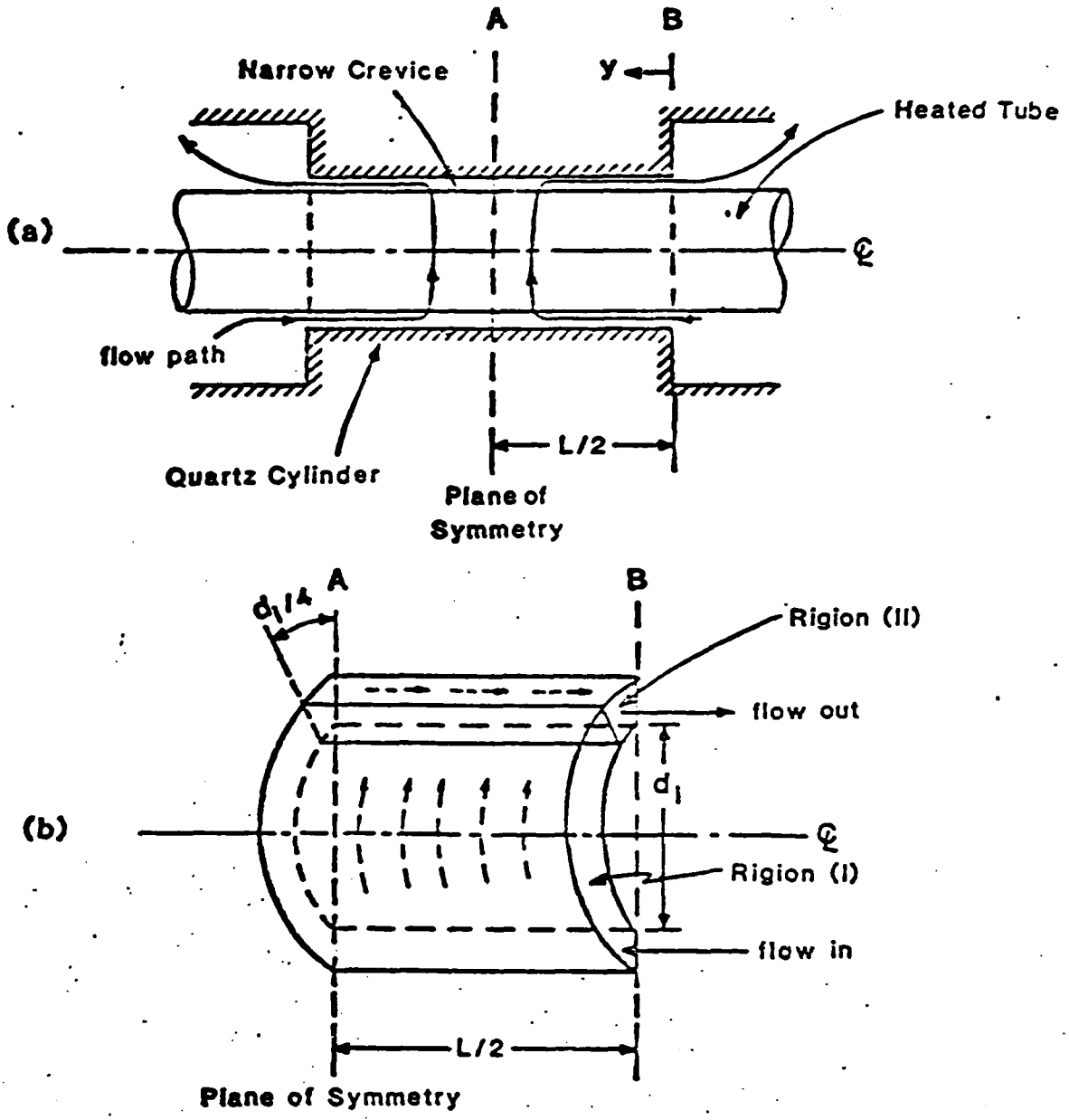
A
B
Narrow Crevice
y
Heated Tube
(a)
℄
flow path
Quartz Cylinder
L/2
Plane of
Symmetry
A
B
d1/4
Rigion (II)
flow out
d1
(b)
℄
Rigion (I)
flow in
L/2
Plane of Symmetry

Fig. 11

Chapter 2

Heat Convection and Fluid Flow in Tube Bundles at Very Low or Very High Reynolds Numbers

Momenclature

a	cylinder radius
b	fluid envelope radius, $(\frac{X_T X_L}{\pi})^{1/2}$
$\bar{C}$, $\bar{D}$	coefficients in eq. (11)
$\bar{E}$, $\bar{F}$	coefficients in eq. (11)
c_2 , c_3	constants in eq. (34)
C_h	nondimensional coefficient, $Re_{D_h}^{0.4}\ Pr^{2/3}\ St$
d	cylinder diameter, 2a
D_h	hydraulic diameter, defined in eq. (2)
D_v	hydraulic diameter, defined in eq. (3)
f	Fanning fraction, defined in eq. (21)
h	heat transfer coefficient
k	thermal conductivity of fluid
Nu_{D_h}, $\overline{Nu}_{D_h}$	local and average Nusselt number
Nu_d, $\overline{Nu}_d$	local and average Nusselt numbers
P	pressure
Pe_d	Peclet number, $Pr\ Re_d$
Pr	Prandtl number, ν/α
r	radial coordinate
Re_d	Reynolds number, Ud/ν
Re_{D_h}	Reynolds number, UD_h/ν
Re^*	modified Reynolds number, defined in eq. (24)
S	solidity, $\pi d^2/[4X_T X_L]$
St	Stanton number
t	nondimensional local fluid temperature, $\frac{T - T_w}{T_b - T_w}$
T	local fluid temperature

T_w	wall temperature
T_b	fluid bulk mean temperature
u	free stream velocity
U	flow velocity at minimum cross-section in bundles
V_r	radial component of fluid velocity
V_θ	θ component of fluid velocity
X_L	longitudinal pitch
X_T	transverse pitch
Z	nondimensional variable, $-\eta^{1/2}/\xi^{1/3}$
α	thermal diffusivity of fluid
β	ratio of cell radius to tube radius, $\frac{b}{a}$
ϵ	voidage, $1 - S$
η	nondimensional stream function, $\frac{\psi}{Ua\lambda}$
θ	coordinate
λ	function of solidity, $\frac{\beta^4 - 1}{(1+\beta^4)\ln\beta^2 + (1-\beta^4)}$
μ	viscosity of fluid
ν	kinematic viscosity of fluid
ξ	variable, defined in eq. (30)
σ_r	radial shear stress component
σ_θ	tangential stress component
ψ, ψ'	stream functiton

ABSTRACT

The empirical formulation of Biery [1], which employed geometric transformation, for the heat transfer in tube bundles at high Reynolds number and cross flow has been extended. A simple heat transfer correlation can be deduced as $\overline{Nu}_d = 0.366\ Re_d^{.6}\ Pr^{1/3}$. This is because the homogenous turbulent mixing in the bundles at high Reynolds number at cross flow the local heat transfer dominates that detail geometry of bundles is no more important.

At very low Reynolds number, the flow streamlines in a bundle are symmestric with respect to a plane separating the upstream and downstream side of a tube. The flow field can be approximated by the "free surface model" togather with creeping flow approach. The calculations show that the pressure drop is dependent upon on the solidity ($1/\beta^2$) and transverse pitch to diameter ratio (X_T/d) of a tube bundle. The Fanning friction factor is described as $f = \frac{8}{Re^*}(\mu_b/\mu_w)^{0.14}$, where $Re^* = Re_d\ [\ \ln \beta^2 + \frac{1-\beta^4}{1+\beta^4}\ ][1 - d/X_T]^{-1}$. This derived equation can predict experimental data of friction factor within ± 20% for Reynolds number Re_d less than 200. For the condition of high Peclet number the average Nusselt number on a tube is derived as $\overline{Nu}_d = 1.185\ \lambda^{1/3}\ Re_d^{1/3}\ Pr^{1/3}\ (\mu_b/\mu_w)^{0.14}$, where $\lambda = \frac{\beta^4 - 1}{(1+\beta^4)\ \ln\beta^2 + (1-\beta^4)}$. Compared with the existing heat transfer data in the range of $Re_d < 200$, a slightly modified coefficient is proposed to fit the data in ± 30%. This gives $\overline{Nu}_d = 0.83\ \lambda^{1/3}\ Re_d^{1/3}\ Pr^{1/3}\ (\mu_b/\mu_w)^{0.14}$.

INTRODUCTION

Extensive studies [1-10] has been conducted for the heat transfer in tube bundles at cross flow due to its wide range of applications. Large quantity of data was presented in reference [10] for heat transfer and pressure drop over smooth tube bundles at high Reynolds numbers. From the designer's view point, there is a need of a general correlation on the prediction of heat transfer coefficients and friction factor of cross flow through tube bundles. Recent, Biery [1] proposed a new method by transforming the actual tube bundle to an equivalent equilateral triangular pitch infinite smooth tube bank (ETP-I-STB) based on the same hydraulic diameter to tube diameter ratio. The heat transfer results is presented in the form of

$$\overline{Nu}_{D_h} = C_h \, Re_{D_h}^{0.6} \, Pr^{1/3} \tag{1}$$

It's found that the transformation had the property of bringing all of the various configurations of tube bundles onto a single curve of C_h vs. $(X_T/d)_\Delta$ (transverse pitch to diameter ratio of ETP-I-STB). The results were compared with published experimental data for bundles with pitch to diameter ratios range from 1.25 to 2.50 and Reynolds numbers Re_{D_h} above 4000. The prediction of C_h for staggered array tube bundles appeared to be quite satisfactory but an error of 20 percent too high existsfor in-line tube bundles. The hydraulic diameter in Biery's study [1] was defined based on the minimum flow cross section area in tube bundle as that of Kays & London [9].

$$D_h = \frac{4 \, (\text{ minimum flow cross section area }) \, (\text{ longitudinal pitch })}{(\text{ heat transfer area })} \tag{2}$$

While in some of the early literatures [2-9] the hydraulic diameter was defined based on the volume of fluid in tube bundles.

$$D_v = 4 \frac{(\text{ free volume })}{(\text{ wetted perimeter })} \quad (3)$$

At low Reynolds number condition, Gunter and Shaw [5] recommended an empirical correlation for the pressure drop of cross flow through tube bundles. The single correlation was generally in good agreement for many tube layouts of interest, but was considerably lower in prediction for the square staggered tube arrangements [3,5]. On the other hand, Ishihara and Bell [11] solved the Navier-Stokes equation, numerically for in-line square tube bundles with pitch to tube diameter ratios range from 1.20 to 2.25 and Reynolds number from 1 to 100. Their results for 1.25 and 1.50 pitch to diameter ratios are in well agreement with experimental data. But no general correlation of friction factor was proposed.

At the low Reynolds number condition, the heat transfer data of staggered tube bundles have been conducted by Whitaker [12]. The correlation is well satisfied with the data of most staggered bundles but can not predict the data of in-line bundles well.

At high Reynolds numbers, it is likely that the tubulent mixing is so substantial that even a simpler formulation than that of Biery [1] can be generated. On ther limit of very low Reynolds numbers, the creeping flow type approximation can be used to derive the formulation of friction factor and heat transfer. This is the objective of this paper to present the results of these studies at extreme Reynolds numbers.

HIGH REYNOLDS NUMBER CONDITIONS

In the transformation approach of Biery [1], the coefficient C_b in bundles was correlated as :

$$C_h = 0.2818\ (X_T/d)_\Delta - 0.1282 - \frac{0.08263\ [\ 1.2 - (X_T/d)_\Delta\ ]}{[(X_T/d)_\Delta - 0.8924\ ]} \qquad (4)$$

Where $(X_T/d)_\Delta = \frac{1}{2}(3.628\ \frac{D_h}{d} + 1)^{1/2}$ is the transverse pitch to diameter ratio of the equivalent equilateral triangular pitch infinite smooth tune bundle (ETP-I-STB), the Reynolds number Re_{D_h} is based on the hydralic diameter D_h of eq. (2) and the flow velocity at minimum flow cross section in bundles.

In fact, the eq. (1) and eq. (4) can be rearranged into a simple expression as

$$\overline{Nu}_d = C_h\ Re_d^{0.6}\ Pr^{1/3}\ (\frac{d}{D_h})^{0.4}$$

$$= \Big\{\ [\ 0.09533 + 0.1409\ (\ 3.628\ \frac{D_h}{d} + 1\ )^{1/2}]$$

$$- \frac{0.034308}{[0.3628\ D_h/d + 1]^{1/2} - 0.9848}\ \Big\}\ Re_d^{0.6}\ Pr^{1/3}\ [\frac{d}{D_h}]^{0.4} \qquad (5)$$

Where $\overline{Nu}_d$ is the average Nusselt number around a tube in the bundles.

Examination of eq. (5) shows an interesting result that $C_h\ (d/D_h)^{0.4}$ is nearly a single value of 0.366 for the tube spacing range from 1.25 to 2.50 as shown in Fig. 1. Thus eq. (5) can be simplified as :

$$\overline{Nu}_d = 0.366\ Re_d^{0.6}\ Pr^{1/3} \qquad (6)$$

Hence, equation (6) gave a simple expression on the heat transfer coefficient of tube bundles in spite of the tube spacing and tube layout in this described range of

conditions. Eq. (6) is compared with various experimental data in Fig. 2. It can be seen that the data tend to fall within ± 20% of eq. (6) for Re_d greater than 4000. It's believed that at high Reynolds number conditions the violent tubulent mixing exists in the bundles such that the local effect at tube wall dominate and the detail geometry of bundle is no more important. However this phenomena breaks down at intermediate Reynolds number conditions as shown in Fig. 2 especially for in-line tube bundles.

LOW REYNOLDS NUMBER CONDITIONS

When the Reynolds number Re_d is low,flow field can be well characterized by creeping flow approximation. At this conditions the flow streamlines are symmetric with respect to a plane which passes through the tube and normal to the incoming stream.

Various investigations [13,14] of creeping flow through packed beds and fluidized beds has been conducted by using "free surface model". The application of this model reduces the complex and difficult problem of the multiparticle assemblage by a set of concentric cells. The model assumes that in this cell a spherical particle is enclosed by a hypothetical fluid envelope. The envelope has zero shear stress at its outer surface. Each cell contain the same amount of fluid as the relative volume of fluid to particle volume in the entire assemblage. The entry and exit effect are neglected in this model. The fluid mechanics study of creeping flow in tube bundles using the "free surface model" has been performed in reference [16]. However no correlation on pressure drop were recommended and no analysis on heat transfer was performanced. In fact, the objective of this study is to provide this information to the readers.

ANALYSIS

Fig. 3 shows the diagrams of the typical staggered array and in-line array tube bundle with the flow normal to the tubes. In the following section the fluid flow and heat convection will be analyzed with the following assumptions.

1. The flow is steady state with constant fluid properties.
2. The fluid is at laminar, creeping flow with negligible energy disspation.
3. The bundles are infinite with negligible entry and exit effects. The tube end effect are also negligible.
4. Cell model is representative for all the geometry of bundles. This assumption will be justified by the comparision of the present results to reported experimental data.

With the use of the "free surface model", the hydrodynamic problem of the bundles is reduced to one of a cylinder with radius a and surrounded by a cylindrical envelope of fluid with a free surface at radius b as shown in Fig 4. The fluid envelope moves as cross flow at a constant velocity U, which is the velocity at the mininum cross section in the tube bundle. The ratio of the cell radius to the tube radius , β, is related to the voidage ϵ of the bundle by

$$\beta = \left(\frac{1}{1 - \epsilon} \right)^{1/2} \tag{7}$$

The β is related to the solidity of a bundle S as $S = \frac{1}{\beta^2}$. The voidage of tube bundle can be also related to the pitch to diameter ratio as

$$\epsilon = \frac{X_T X_L - \pi d^2 / 4}{X_T X_L} \tag{8}$$

Therefore one gets :

$$b = \left(\frac{X_T X_L}{\pi} \right)^{1/2} \tag{9}$$

This is the relationship between the tube bundles pitch X_T, X_L with the unit cell radius b in the free surface model.

FLUID FLOW

Formulation. For simplicity of derivation, the cylinder of radius a is assumed to moves perpendicular to its axis in a fluid cell of radius b as shown in Fig. 4. The momentumn equation of creeping flow with inertia terms neglected can be written in term of stream function.

$$\nabla^4 \psi' = 0 \tag{10}$$

The general soluton for eq. (10) is found as :

$$\psi'(r,\theta) = \sin\theta \left[\bar{C} r^3 + \bar{D} r \ln r + \bar{E} r + \frac{\bar{F}}{r} \right] \tag{11}$$

The boundary conditions in the cell model are [12]:

$$\left.\begin{aligned} V &= U \\ V_r &= U \cos\theta \\ V_\theta &= U \sin\theta \end{aligned}\right\} \quad \text{at } r = a$$

$$\left.\begin{aligned} V_r &= 0 \\ \frac{\partial V_\theta}{\partial r} &+ \frac{1}{r}\frac{\partial V_r}{\partial \theta} - \frac{V_\theta}{r} = 0 \end{aligned}\right\} \quad \text{at } r = b \tag{12}$$

Theses conditions are based on the no–slip conditions on the cylinder together with the zero shear stress conditions at the outer surface of the unit cell. They provides the simulataneous equations to evaluate the constants in equation (11).

$$\bar{C} = \frac{a^2}{2}\,\frac{U}{(a^4+b^4)\,\ln(a/b) + 0.5\,(a^4 - b^4)}$$

$$\bar{D} = \frac{-U}{\ln(b/a) + a^4/(a^4+b^4) - (1/2)}$$

$$\bar{E} = \frac{U \ln b}{\ln(b/a) + (a^4-b^4)/2(a^4+b^4)}$$

$$\bar{F} = \frac{-U\,a^2\,b^4}{2(a^4+b^4)\,\ln(b/a) + (a^4 - b^4)} \tag{13}$$

Therefore, the stream function is

$$\psi'(r,\theta) = \frac{\lambda\, r\, U \sin\theta}{(\beta^4 - 1)}\left(\frac{r^2}{a^2} + 2\,(1+\beta^4)\,\ln(b/r) - \frac{\beta^4 a^2}{r^2}\right) \tag{14}$$

To obtain the velocity component V_r and V_θ on the basis that the inner cylinder is stationary and that the fluid envelope is moving with the constant velocity U, one simply needs to add $-U\cos\theta$ to V_r and $U\sin\theta$ to V_θ which can be derived from eq. (14). Therefore, the correspondingly stream function becomes

$$\psi = \psi' - r\,U\sin\theta$$

$$= \frac{\lambda\,U\,r\sin\theta}{(\beta^4-1)}\left(\frac{r^2}{a^2} + 2(1+\beta^4)\ln(a/r) - (1-\beta^4) - \frac{\beta^4a^2}{r^2}\right) \qquad (15)$$

and

$$V_r = \frac{\lambda\,U\cos\theta}{(\beta^4-1)}\left(\frac{r^2}{a^2} + 2(1+\beta^4)\ln(b/r) - \frac{\beta^4a^2}{r^2}\right) - U\cos\theta$$

$$V_\theta = \frac{-\lambda\,U\sin\theta}{(\beta^4-1)}\left(3\frac{r^2}{a^2} - 2(1+\beta^4)(\ln r + 1) + 2(1+\beta^4)\ln b\right.$$

$$\left. + \frac{\beta^4a^2}{r^2}\right) + U\sin\theta \qquad (16)$$

Where $\lambda = \dfrac{\beta^4 - 1}{(1+\beta^4)\ln\beta^2 + (1-\beta^4)}$, which decreased with increasing solidity $1/\beta^2$.

Drag Force. Attention is drawn here upon the magnitude of the pressure gradient in tube bundles which is of great importance in practice. The method given in [15]

was used to calculate the drag force on a cylinder from the knowledge of stream function by integrating the surface force around the surface.

$$F_D = \int_0^{2\pi} (\sigma_r \cos\theta - \sigma_\theta \sin\theta)\, a^2\, d\theta \tag{17}$$

where σ_r and σ_θ represent the radial and tangential stress component and defined as :

$$\sigma_r = - p + 2\mu \frac{\partial V_r}{\partial r}$$

$$\sigma_\theta = \mu \left(\frac{\partial V_\theta}{\partial r} - \frac{V_\theta}{r} + \frac{1}{r} \frac{\partial V_r}{\partial r} \right) \tag{18}$$

Substituting V_r , V_θ from eq. (16) into eq. (18) and (17), eventually one gets

$$F_D = \frac{- 8\, \pi\, \mu\, a\, U\, (\beta^4 + 1)\, \lambda}{(\beta^4 - 1)} \tag{19}$$

The force per unit length associated with a single cell may be related to the pressure gradient in tube bundles. Hence,

$$\frac{F_D/2a}{\pi b^2} = \frac{dp}{dx} \tag{20}$$

The Fanning friction factor f is defined in term of the pressure gradient and hydraulic diameter [15] by the following equation.

$$(-\frac{dp}{dx}) = 4 f \bullet \frac{1}{D_h} \bullet \frac{\rho U^2}{2} \tag{21}$$

As mention early, two different definition of hydraulics diameter were made by several investigators. Use the definition of eq. (2) following Kays and London [10].

$$\frac{D_h}{d} = \frac{4}{\pi} \left(\frac{X_T}{d} - 1 \right) \frac{X_L}{d}$$

$$= \beta^2 - \frac{X_L\, d}{(\pi d^2/4)} \tag{22}$$

In the present study, the definition of hydrodynamic diameter in eq. (22) is found to be superior than the one following eq. (3) in correlating the data. The equation (19) to (22) can be rearrange to give

$$f = \frac{8}{Re^*} \tag{23}$$

Where the modified Reynopids number Re^*, which is related to the bundle geometry, is defined as :

$$Re^* = Re_d \left[\ln \beta^2 + \frac{(1-\beta^4)}{(1+\beta^4)} \right] \left(1 - d/X_T \right)^{-1} \tag{24}$$

To account for the property change of fluid at heating or cooling, a correction factor [2] $\left(\frac{\mu_b}{\mu_w} \right)^{0.14}$ is applied in eq. (23). Finally, the friction factor is becomes

$$f = \frac{8\,(\beta^4+1)\,(1 - d/X_T)}{Re_d\,[\,2(\beta^4+1)\,\ln\beta + (1-\beta^4)\,]} \left(\frac{\mu_b}{\mu_w}\right)^{0.14} \qquad (25)$$

Where μ_b and μ_w are the fluid viscosity evaluated at T_b and T_w respectively.

Discussion. The calculated Fanning friction factor, eq. (25), is plotted in Fig. 5 versus tube Reynolds number for flow across in-line square tube bundles at different pitch to diameter ratio. Comparision is made with Bell's numerical solution [10] and published experimental data [3,6,7]. It appears that the Fanning friction factor increased as pitch to diameter ratio decreased and decreased with increasing Reynolds number. Present results are in well agreement with the experimental data and Bell's solution at p/d = 1.25, 1.5 at various Reynolds numbers. It's also noticed that the creeping flow results is only slightly effected by inertia for Re_d below 200.

Further comparision of the pressure drop data for bundles with various tube arrangement is shown in Fig. 6 where the calculated fricton factor is plotted versus the modified Reynolds number Re^*. All the available data tend to lie within ± 20% of the present study for $Re^* < 400$. When the modified Reynolds number is greater than 400, turbulence probably appears in various degree in the tube bundles, and the creeping flow approach under-predicts the pressure drop in tube bundles. Although eq. (25) is more complicated than Gunter and Shaw's correlation [5], the present correlation appears to be a somewhat better one because it fits all the data for $Re_d < 200$, while Gunter and Shaw's correlation predicted 50% low values for staggered bundles with square tube layout [9].

HEAT TRANSFER

Formulation. Although the present analysis is retricted to the creeping flow, at large Peclet number the boundary layer will be very thin and stays close to the surface of the heated tube. For a thin boundary layer, $r \cong a$, then the stream function of eq. (15) can be expanded by Taylor's series and reduced to

$$\psi \cong \frac{-2\lambda U \sin\theta\,(r-a)^2}{a} \tag{26}$$

Neglect the viscous dissipation, the energy equation in the unit cell becomes :

$$V_r \frac{\partial T}{\partial r} + V_\theta \frac{\partial T}{r\partial\theta} = \alpha \left(\frac{\partial^2 T}{\partial r^2} + \frac{1}{r}\frac{\partial T}{\partial r} \right) \tag{27}$$

with constant wall temperature boundary :

$$T = T_w \quad \text{at} \quad r = a$$

$$T = T_b \quad \text{at} \quad r = b$$

The energy equation can be transformed to its nondimensional form by introducing the dimensionless quantities :

$$\eta = \frac{\psi}{Ua\lambda}$$

$$= -2\left(\frac{r-a}{a}\right)\sin\theta \tag{28}$$

$$t = \frac{T - T_w}{T_b - T_w}$$

Due to the thin boundary layer $(r-a)/a \ll 1$, $\frac{\partial^2 T}{\partial r^2} \gg \frac{1}{r}\frac{\partial T}{\partial r}$. The second term at the right side of eq. (27) is negligible. The steady state convective-diffusion equation, therefore, can be rewritten in the form of

$$\frac{\partial t}{\partial \theta} = \frac{4\ (2\ \sin\theta)^{1/2}}{Pe_d\ \lambda}\ \frac{\partial}{\partial \eta}\left(\ (-\eta)^{1/2}\ \frac{\partial t}{\partial \eta}\ \right) \tag{29}$$

where

$Pe_d = \frac{2\ U\ a}{\alpha}$ is the Peclet number

Using the new variable

$$\xi = \frac{4\ (2)^{1/2}}{Pe_d\ \lambda}\int_0^{\theta} \sin\theta^{1/2}\ d\theta \tag{30}$$

eq. (29) becomes

$$\frac{\partial t}{\partial \xi} = \frac{\partial}{\partial \eta}\left(\ (-\eta)^{1/2}\ \frac{\partial t}{\partial\ \eta}\ \right) \tag{31}$$

Eq. (31) can be further simplified by introducing the similarity variable Z.

$$Z = \frac{(2\ \sin\theta)^{1/2}\ y\ (Pe_d\ \lambda)^{1/3}}{a\ (4\ (2)^{1/2})^{1/3}}\ (\int_0^{\theta} (\sin\theta)^{1/2}\ d\theta)^{-1/3} \tag{32}$$

The governing eq. can be trasnsferred into the ordinary differential equation.

$$\frac{d^2t}{dZ^2} + \frac{4}{3} Z^2 \frac{dt}{dZ} = 0 \tag{33}$$

Eq. (33) can be integrated twice :

$$t(Z) = c_2 \int_0^Z e^{-\frac{4}{9}Z^3} dZ + c_3 \tag{34}$$

The constant c_2, c_3 can be evaluated from boundary conditions

(i) at $r = a$, $t = 0$, therefore

$c_3 = 0$

(ii) at $r = b$, ($\eta \to \infty$, $Z \to \infty$) , $t = 1$, therefore

$$c_2 = \left(\int_0^{\infty} e^{-\frac{4}{9} Z^3} dZ \right)^{-1}$$

The second boundary condition is rewritten as that the stream function at the outer surface of the unit cell approach infinite. This is reasonable since the quantity (b–a) is always much greater than the thermal boundary layer thickness at High Peclet number conditions. Finally, one can get

$$t = \frac{T - T_w}{T_b - T_w} = \frac{\int_0^Z e^{-(4/9)Z^3} dZ}{(9/4)^{1/3} \Gamma(4/3)} \tag{35}$$

<u>Nusselt Number.</u> The local Nusselt number based on the hydraulic diameter is obtained from the equaton.

$$Nu_{D_h} = \frac{h\, D_h}{k}$$

$$= \frac{-\, k\, (\partial T/\partial r)\big|_{r=a}}{(k/D_h)\, \Delta T} \qquad (36)$$

Substituting eq. (35) into eq. (36) yields :

$$Nu_{D_h}\,(\theta,\, Pe_d) = \frac{(16\, Pe_d\, \lambda)^{1/3}\, (\sin\theta)^{1/2}}{\Gamma(4/3)} \left(9 \int_0^{\theta} (\sin\theta)^{1/2}\, d\theta \right)^{-1/3} (\, D_h/d\,)$$

Therefore, the local Nusselt number based on the tube diameter can be written as :

$$Nu_d\,(\theta,\, Pe_d) = \frac{h\, d}{k}$$

$$= \frac{(16\, Pe_d\, \lambda)^{1/3}\, (\sin\theta)^{1/2}}{\Gamma(4/3)} \left(9 \int_0^{\theta} (\sin\theta)^{1/2}\, d\theta \right)^{-1/3} \qquad (37)$$

In this equation the dependence of the heat transfer coefficient on the hydraulic diameter of cross flow in tube bundles disappears. The average Nusselt number $\overline{Nu_d}$ is evaluated by integrating the local Nusselt number around the tube .

$$\overline{Nu_d} = 1.185\, Re_d^{1/3}\, \lambda^{1/3}\, Pr^{1/3} \qquad (38)$$

The correction fractor $\left(\frac{\mu_b}{\mu_w} \right)^{0.14}$ is also proposed here to account for the properities change. Therefore, the average Nusselt number becomes :

$$\overline{Nu}_d = 1.185\ Re_d^{1/3}\ \lambda^{1/3}\ Pr^{1/3} \left(\frac{\mu_b}{\mu_w} \right)^{0.14} \tag{39}$$

Equation (39), therefore, give an analytical relationship between the heat transfer coefficient and Reynolds number for tube bundles of any regular geometry with the solidity ($\frac{1}{\beta^2}$) of the tube bundle as a parameter.

Discussion. The present solution is restricted to low Reynolds number and high Peclet number. Fig. 7 shows the comparision of eq. (39) and data in term of $\frac{\overline{Nu}_d}{Pr^{1/3}\ (\mu_b / \mu_w)^{0.14}}$ versus $\lambda\ Re_d$ for various tube arrangement. We may also note that the data of which natural convection is significant [16,17] are excluded in present analysis. The eq. (39) over-predicts the data, this is possible because the range of Reynolds number of the data base is larger than the range of the creeping flow that the flow streams are, in fact, non-symmtric for the upstream and downstream portion with respect to the tube. The analysis is assuming creeping flow gives a symmetric stream lines which, therefore, over-predicts the heat transfer. In order to fit the data base in this Reynolds number range, it is suggested that the constant in eq. (39) is reduced. That suggests

$$\overline{Nu}_d = 0.83\ \ Re^{*\ 1/3}\ Pr^{1/3}\ \lambda^{1/3} \left(\frac{\mu_b}{\mu_w} \right)^{0.14} \tag{40}$$

All the data fall within ± 30% of this semi-empirical correlation. Eq. (40) contains a term λ which is dependent upon the tube spacing. The increasing of the tube spacing results in lower heat transfer coefficient. In other words, the solidity ($\frac{1}{\beta^2}$) plays an important role in the performance of cross flow in tube bundles at low Reynolds number high Peclet number conditions.

To compare in a comon base it is found that Whitaker's correlation [12] can be reformed in a similar form.

$$\overline{Nu}_d = 1.526\ Re_d^{1/3}\ (\beta^2 - 1)^{-2/3}\ Pr^{1/3} \left(\frac{\mu_b}{\mu_w} \right)^{0.14} \qquad (41)$$

Equation (41) and (40) are compared with experimental data in Fig. 8 for the effects of β^2. Both eqs. show the tendence of increasing the heat transfer coefficient by increasing the solidity ($1/\beta^2$) of the bundles. The comparison indicates that the present semi-empirical correlation, eq. (40), is slightly better than the empirical correlation of Whitaker's.

CONCLUSION

The empirical formulation of Biery [1], which employed geometric transformation, for the heat transfer in tube bundles at high Reynolds number and cross flow has been extended. A simple heat transfer correlation can be deduced as shown in eq. (6). This is because the homogenous turbulent mixing in the bundles at high Reynolds number at cross flow the local heat transfer dominates that detail geometry of bundles is no more important. However this phenomena breaks down at intermediate Reynolds number as shown in Fig. 2. Eq. (6) give a satisfied prediction of ± 20% error compared with the experimental data for Reynolds number above 4000.

At very low Reynolds number, the flow streamlines in a bundle are symmestric with respect to a plane separating the upstream and downstream side of a tube. The flow field can be approximated by the "free surface model" togather with creeping flow approach. The calculations show that the pressure drop is dependent upon on the

solidity ($1/\beta^2$) and transverse pitch to diameter ratio (X_T/d) of a tube bundle. The Fanning friction factor is proposed as shown in eq. (25). This derived equation can predict experimental data of friction factor within ± 20% for Reynolds number Re_d less than 200.

For the condition of high Peclet number the average Nusselt number on a tube is derived as $\overline{Nu}_d = 1.185\ \lambda^{1/3}\ Re_d^{1/3}\ Pr^{1/3}\ (\mu_b/\mu_w)^{0.14}$, where λ is a function of the solidity. Compared with the existing heat transfer data in the range of $Re_d < 200$, a slightly modified coefficient is proposed to fit the data in ± 30%. This gives $\overline{Nu}_d = 0.83\ \lambda^{1/3}\ Re_d^{1/3}\ Pr^{1/3}\ (\mu_b/\mu_w)^{0.14}$.

REFERENCES

1. Biery, J. C., "Prediction of Heat Transfer Coefficients in Gas Flow Normal to Finned and Smooth Tube Banks," J. of Heat Transfer, 1981, pp. 705-714.

2. Omohundro, Q. A., Berglin, O. P. and Colburn, A. P., "Heat Transfer and Fluid Friction During Viscous Flow Across Banks of Tubes", Trans. ASME, 1949, pp. 27-34.

3. Bergelin, O. P., Colburn, A. P. and Hull, H. C., "Heat Transfer and Fluid Friction During Flow Across Banks of Tubes," University of Delaware, Eng. Exp. Station Bull. No. 2, 1950.

4. Bergelin, O. P., Davis, E. S. and Hull, H. C., "A Study of Three Tube Arrangements in Unbaffled Tubular Heat Exchangers," Trans. ASME, Vol. 71, 1949, pp. 367-374.

5. Gunter, A. Y. and Shaw, W. A., "A General Correlation of Friction Factors For Various Types of Surface of Cross Flow," Trans. ASME, Vol. 67, 1945, pp. 643-660.

6. Chilton, T. H. and Generaux, R. P., "Pressure Drop Across Tube Banks," Trans. AIChE, Vol. 29, 1933, pp. 161-173.

7. Sieder, E. N. and Scott, N. A., "Fluid Friction at Parallel and Right Angles to Tubes and Tube Bundles," ASME paper No. 83, 1932.

8. Pierson, O. L., "Experimental Investigation of The Influence of Tube Arrangement on Convection Heat Transfer and Flow Resistance in Cross Flow of Gases Over Tube Banks," Trans. ASME, 1937, pp. 563-572.

9. Bergelin, O. P., Brown, G. A. and Sullivan, F. W., "Heat Transfer and Fluid Friction During Viscous Flow Across Banks of Tubes," Trans. ASME, 1950, pp. 881-888.

10. Kays, W. and London, A. L., COMPACT HEAT EXCHANGER , Macgraw-Hill Co., 1964.

11. Ishihara, k. and Bell, k., "Friction Factor for In-Line Square Tube Bank at Low Reynolds Number," AIChE SYMPOSIUM, 1972, pp. 74-80.

12. Whitaker, S., "Forced Convection Heat Transfer Correlation for Flow in Pipes, Past Flat Plates, Single Cylinders, Single Spheres, and Flow in Packed Beds and Tube Bundles," AIChE J,. Vol. 18, 1972, pp. 361-371.

13. Happel, J., "Viscous Flow Relative to Arrays of Cylinders," AIChE J., 1959, pp. 174-177.

14. Pfeffer, R., "Heat and Mass Transfer in Multipartical System," Ind. Eng. Chem. Fund., 1964, pp. 380-383.

15. Yuan, S. W., FOUNDATION OF FLUID MECHANICS , Prentice-Hall Inc., N.J., 1972.

16. Dennis, S. C. R., "Steady Laminar Forced Convection From a Cylinder at Low Reynolds Numbers," Physics of Fluid, 1968, pp. 933-940.

17. Collis, D. C. and Williams, M. J., "Two-Dimensional Convection From Heated Wires at Low Reynolds Number," J. of Fluid Mechanics, 1970, pp. 17-31.

List of Figures

X_L/d
X_T/d
1.25
1.25 1.5 1.75 2.0 2.25 2.50
1.50
2.0
2.5
"
$C_h \cdot \left(\frac{d}{D_h}\right)^{0.4}$
0.50
0.45
0.40
0.366
0.35
0.30
0.25
$C_h \left(\frac{d}{D_h}\right)^{0.4} \doteq 0.366$
1
2
3
4
5
6
7
β^2

FIG 1

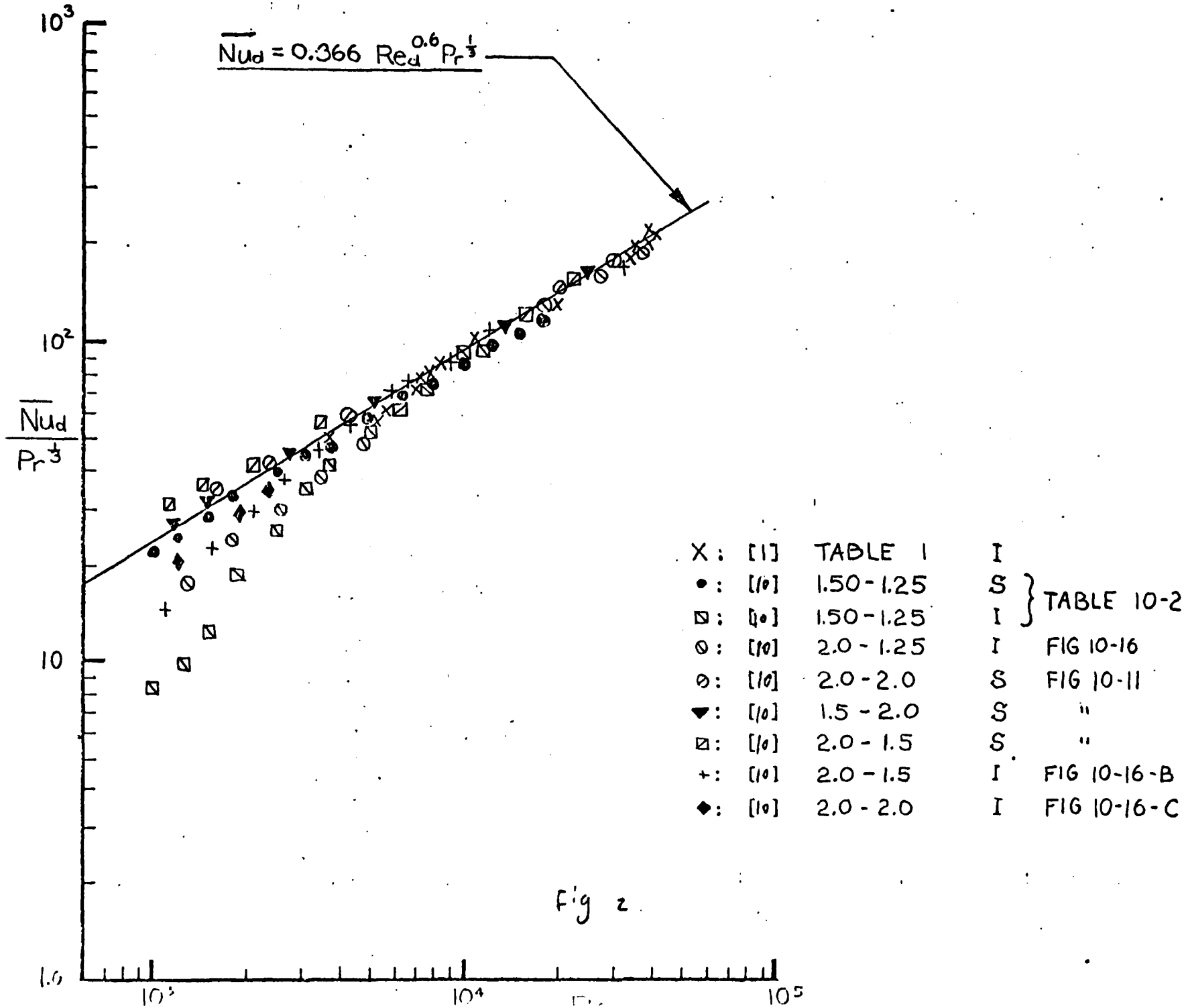
$\overline{Nu_d} = 0.366\ Re_d^{0.6} Pr^{\frac{1}{3}}$
$\frac{\overline{Nu_d}}{Pr^{\frac{1}{3}}}$
10^3
10^2
10
1.0
10^3
10^4
10^5
X : [1] TABLE 1 I
• : [10] 1.50 - 1.25 S } TABLE 10-2
▧ : [10] 1.50 - 1.25 I }
⊙ : [10] 2.0 - 1.25 I FIG 10-16
⊘ : [10] 2.0 - 2.0 S FIG 10-11
▼ : [10] 1.5 - 2.0 S "
▨ : [10] 2.0 - 1.5 S "
+ : [10] 2.0 - 1.5 I FIG 10-16-B
◆ : [10] 2.0 - 2.0 I FIG 10-16-C

Fig 2

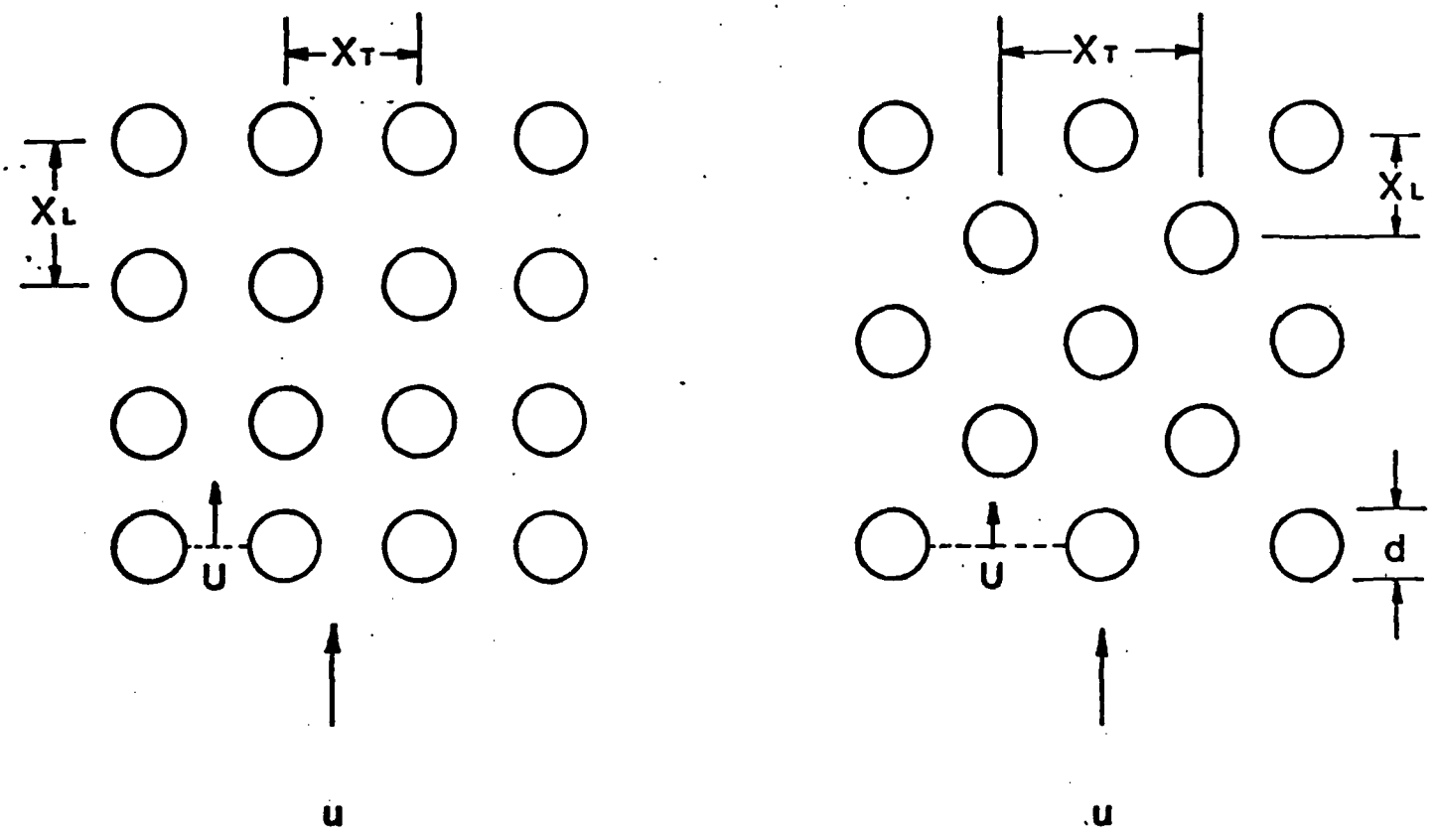

(a) In- Line

(b) Staggered

Fig. 3 Layout of Tube Bundles

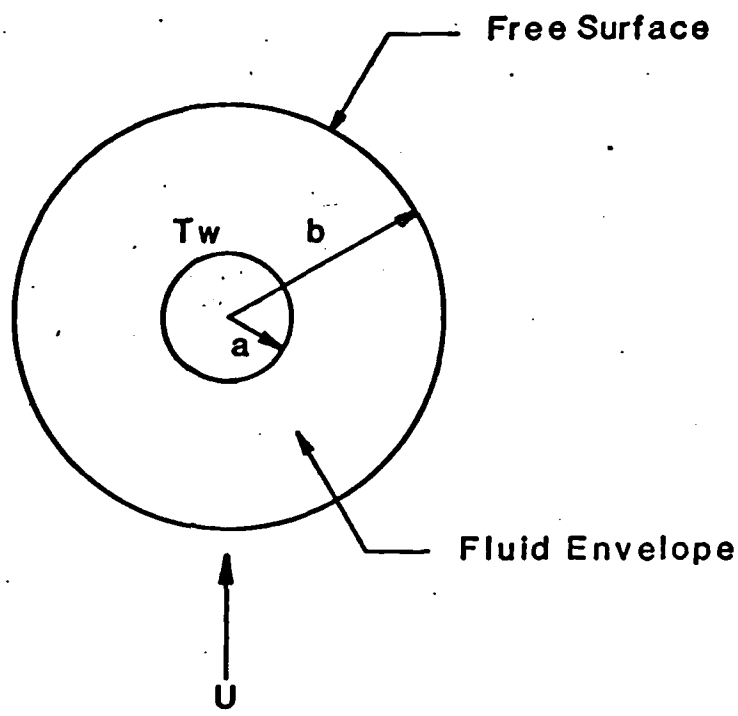

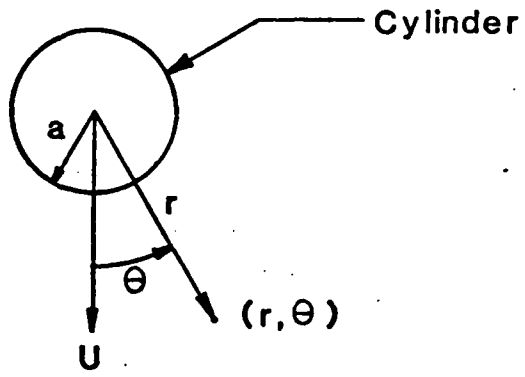

Fig.4 Free Surface Model

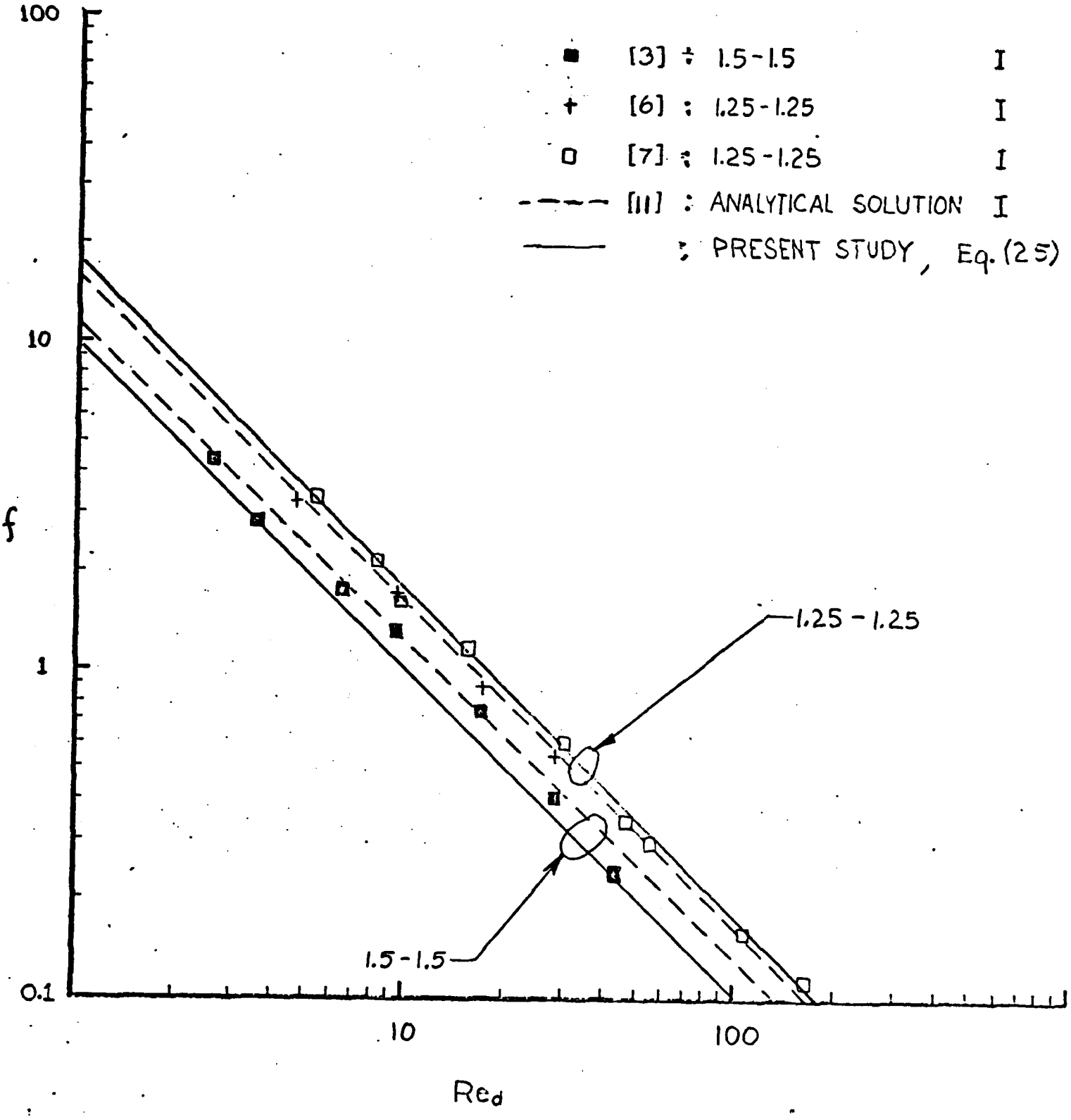
100
10
1
0.1
f
10
100
Re_d
[3] ÷ 1.5-1.5 I
[6] : 1.25-1.25 I
[7] : 1.25-1.25 I
[11] : ANALYTICAL SOLUTION I
: PRESENT STUDY, Eq. (25)
1.25 - 1.25
1.5 - 1.5

FIG 5

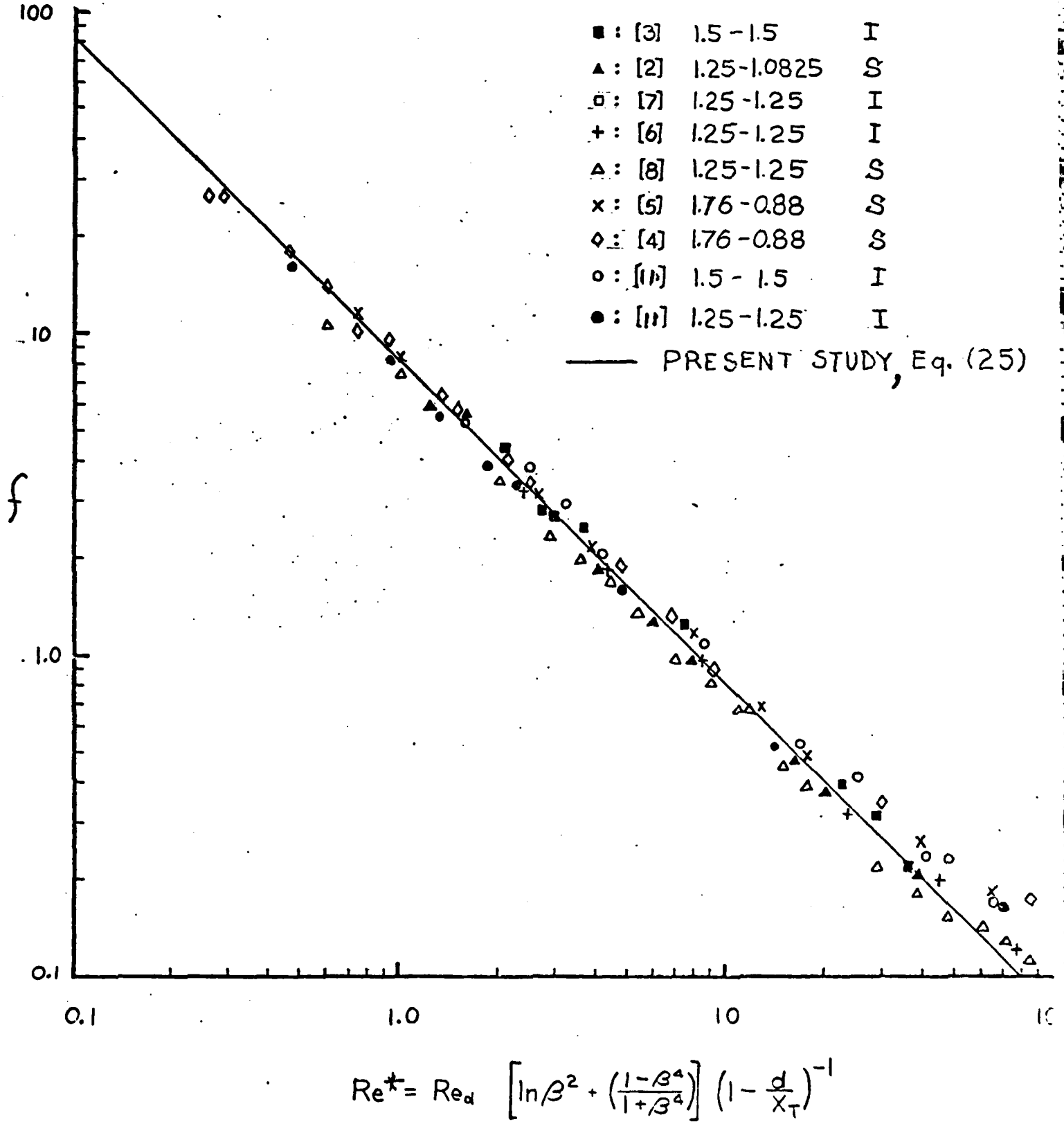

$$Re^{*} = Re_{d} \left[\ln \beta^{2} + \left(\frac{1-\beta^{4}}{1+\beta^{4}} \right) \left(1 - \frac{d}{X_{T}} \right)^{-1} \right]$$

FIG 6

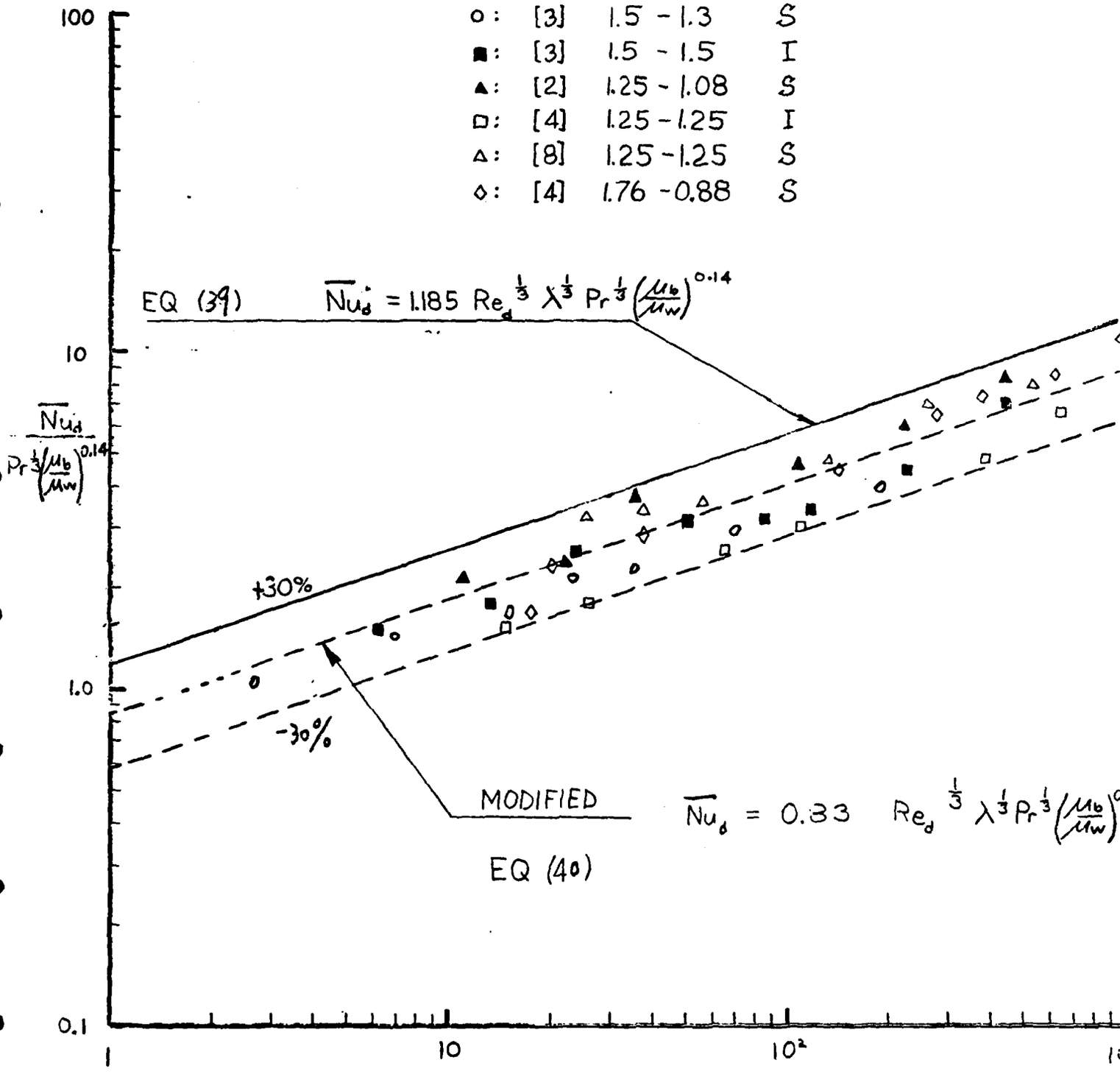
o : [3] 1.5 - 1.3 S
■ : [3] 1.5 - 1.5 I
▲ : [2] 1.25 - 1.08 S
□ : [4] 1.25 - 1.25 I
△ : [8] 1.25 - 1.25 S
◇ : [4] 1.76 - 0.88 S
EQ (39) $\overline{Nu_d} = 1.185\ Re_d^{\frac{1}{3}}\ \lambda^{\frac{1}{3}}\ Pr^{\frac{1}{3}}\left(\frac{\mu_b}{\mu_w}\right)^{0.14}$
100
10
1.0
0.1
$\frac{\overline{Nu_d}}{Pr^{\frac{1}{3}}\left(\frac{\mu_b}{\mu_w}\right)^{0.14}}$
+30%
-30%
MODIFIED
EQ (40)
$\overline{Nu_d} = 0.33\ Re_d^{\frac{1}{3}}\ \lambda^{\frac{1}{3}} Pr^{\frac{1}{3}}\left(\frac{\mu_b}{\mu_w}\right)^{0.}$
1
10
10^2
$Re_d\ \lambda$

FIG 7

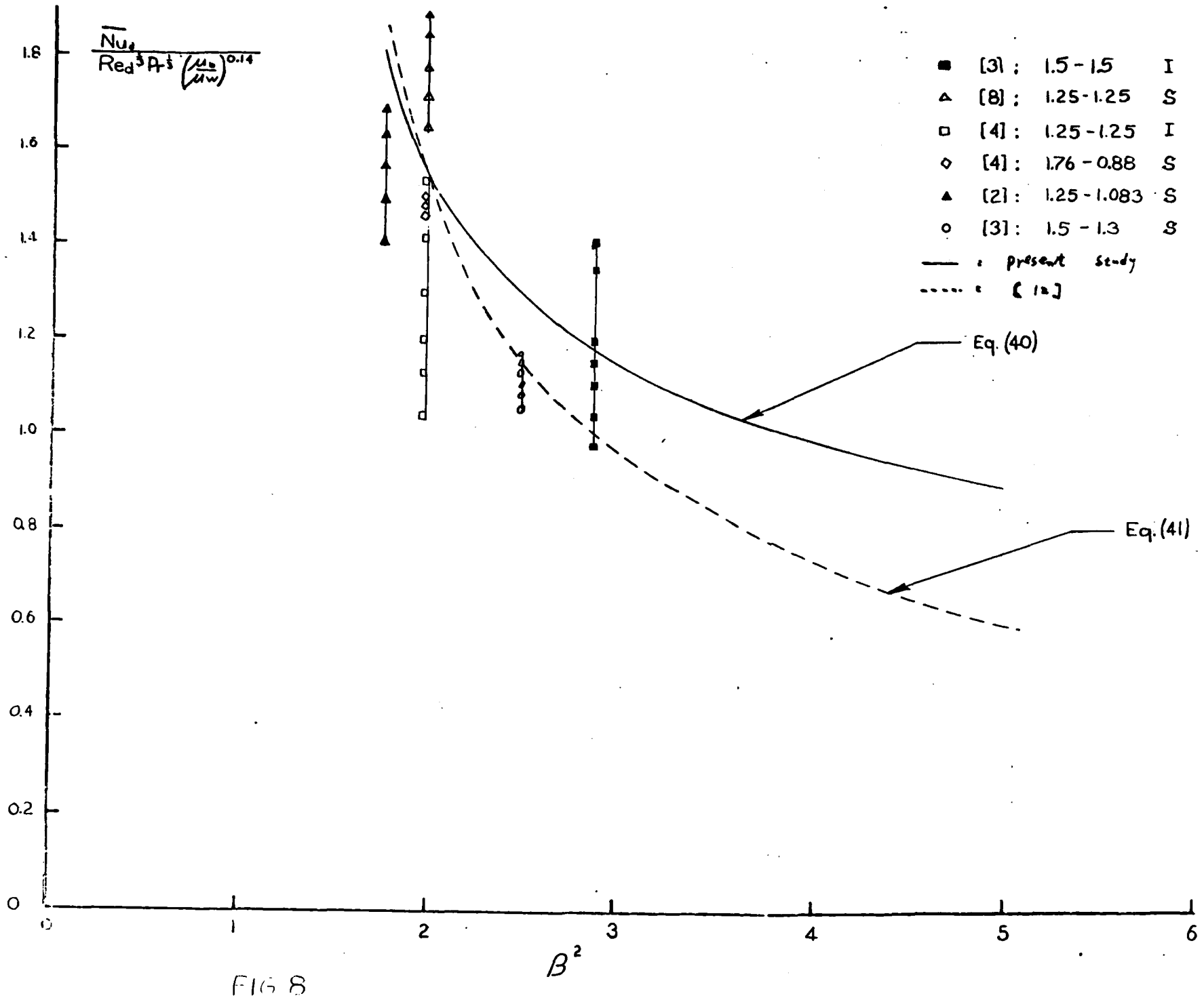
$\frac{\overline{Nu_d}}{Re_d^{\frac{1}{3}} Pr^{\frac{1}{3}} \left(\frac{\mu_b}{\mu_w}\right)^{0.14}}$
[3] ; 1.5 - 1.5 I
[8] ; 1.25 - 1.25 S
[4] ; 1.25 - 1.25 I
[4] ; 1.76 - 0.88 S
[2] ; 1.25 - 1.083 S
[3] ; 1.5 - 1.3 S
: present study
: [12]
Eq. (40)
Eq. (41)
1.8
1.6
1.4
1.2
1.0
0.8
0.6
0.4
0.2
0
0
1
2
3
4
5
6
β^2

FIG 8

Chapter 3

Cross Flow Boiling Heat Transfer in Tube Bundles

INTRODUCTION

Boiling heat transfer in tube bundles has been extensive investigated for many years due to various engineering application. This problem is important in the design of nuclear reactor, evaporator, condenser, chemical reboiler and many major components in chemical and thermal power plants.

Boiling heat transfer can be divided into two categories : pool boiling (where the tube bundle is submerged in an stagnant pool) and flow (forced convection) boiling (in which fluid flow in the heated tube bundle). Estimation of boiling heat transfer, CHF and pressure drop on the outside of tube bundles is one of the important factor in successful design of heat exchanger or steam generator.

Most of previous investigation [1–6] however, were concerned with the axial flow along tube bundles. As a matter of fact, in many thermal system the steam generator and evaporator contain tube bundles which are oriented horizontally. The flow direction is normal to the axial of the tubes and boiling occurs in the shell side as shown in Fig. 1. The tubes can be arranged in in-line or staggered array with a particular pitch to diameter ratio, which determines the tube to tube distance. Steam and water flows by the gravity induced natural convection. However, at any position in the bundle the boiling heat transfer on the tube is mainly dependent upon the local flow velocity and the local quality. The study of heat transfer in a particular region of a large bundle can, therefore, be performed in a smaller bundle at a forced convective boiling condition with the same velocity and quality environment.

Reliable prediction of heat transfer, CHF and pressure drop is vital in optimiming the heat exchanger design. Unfortunately, the knowledge of the hydraulic and boiling

heat transfer in tube bundles at cross flow condition is very inadequate. Extensive reviews on heat transfer of single-phase cross flow in tube bundles are presented in reference [7-16] In two-phase flow case, the vapor bubble distribution affects the flow field and it can't be handled by the well known knowledge of single-phase flow in tube bundles.

Fundamental understanding and parametric effect has been fairly well established for the boiling heat transfer and CHF of a single tube at cross flow condition in reference [17-21]. The major difference between the single tube heat transfer and the heat transfer on a tube in a heated tube bundle is the different flow field and quality environment near the tube surface.

The available information of cross flow boiling heat transfer in tube bundles is mainly oriented from the experience of the reboiler design in chemical process [21-26] and the evaporator design [27-29]. No adequate data exist in the literature for the effect of quality and velocity on the critical heat flux in tube bundles. The peripheral variation of heat transfer coefficient on the heated tube in single tube or bundles are also not available in published literature.

It's also interesting to study the staggered array bundle because the flow streaming phenomena (see Fig. 1.b) may not occurs in staggered array. Therefore, the heat transfer coefficient could be higher because most of the tube surface area would be active. The comparision of boiling heat transfer in staggered array bundle with that in in-line array bundle is still not clear up to now. For a better understanding of boiling heat transfer in tube bundles, a systematical study is required to bridge the well known single tube knowledge to tube bundles. Two tubes or three tubes study [28-29] has served as a base for the study of tube bundles.

The objective of the present investigation is to bridge the knowledge of heat transfer on single tube to the tube bundles, and to compare the heat transfer of tube bundles with staggered array and in-line array. The effect of the thermal environment of a tube in a bundle can also be revealed by comparing the heat transfer results of only one tube heated vs. all tubes heated, and single phase flow vs. two phase flow. With the better understanding on the boiling heat transfer and two phase flow, the computation of the thermal hydraulics in steam generator bundles may become possible.

The major effort in the past year is to fabricate and assembly the test section and the test loop. At the same time, the analysis of single phase foced convection in various tube bundles at very low or very high Reynolds number has been completed. This analysis was presented in the chapter 2 of this report. The experimental set up will be reported in the following section.

EXPERIMENTAL APPARATUS

The major components of the experimental apparatus are : a Freon-113 loop, test section, power supply system, instrumentation system and photographic equipment. All of these components will be described in detail in the following sections.

Freon Loop

The Freon-113 loop in Thermal Science Lab. at Carnegie-Mellon University was modified to achieve a wide range of operation condition. The schematic of the modified loop is presented in Fig. 2 with its specifications described in Table 1.

All parts of the main flow system are constructed of type 304 stainless steel and

insulated with fiber glass. Freon-113 is circulated by a Crane stainless leakage-proof dynapump, model JB-3K, which provides a discharge pressure of 80 psig at 30 GPM. After the pump, the flow is divided into the by-pass line and the test section line. In the test section line , fluid flows through the turbine flow meter, the preheaters, the main regulating valve, and the test section. After the test section, the fluid merges with the flow from the by-pass line. The mixed flow then goes through the condenser, degassing tank, and then flows back to the pump. Two Grainger filters are installed in parallel at by-pass suction line of the pump.

The flow rate through the test section is adjusted by the valve at by-pass line and the valve at the inlet of the test section. The desired system pressure is maintained by the Nitrogen gas in the accumulator. Pump operation is controlled also by the regulating valve at the outlet of the pump. The main regulating valve (1.5 inches diameter), which is located at the entrance of the test section, is used to regulate the two phase quality into the test section. Therefore, the inlet condition to test section will be controlled by varying the power delivered to Freon-113 in the preheaters and the throttling at the main regulating valve before test section.

The preheater system consists of four Chromalox heaters which has the capability of producing a total of 30 KW of power. The first and second preheater are Model ARMTO-3605T2, each with a rated output of 6 KW at 240 V. The third and fourth preheater are Model MTO-390A of 9 KW each. Each preheater is able to provide a continuously variable power using variacs. The preheaters are arranged in a way to prevent the burn out by trapped bubbles on the heaters The second preheater is laid at the top of first preheater. The fourth preheater is installed above the third one with a 10 degree inclination. A separate valve on top of the second preheater is also used to bleed the trapped air in preaters.

The condenser is of a shell-and-tube type with Freon-113 flowing in the shell side and cooling water at the tube side. The valve on the water line is able to control the temperature of Freon-113 before the pump inlet. After the condenser, Freon-113 enters the degassing tank, which is located at the highest point of system.

A photograph of the loop assembly is shown in Fig. 3. The range of parameters for operation conditions in present study is shown in Table 2.

Test Section

The test section under investigation contains the bottom plenum, test bundle and top plenum. The tubes in the test bundle can be reused, the test section casing, inlet plenum and exit plenum are the same in all the tests.

The schematics of the test section is indicated in Fig. 4 with its photograph presented in Fig. 5. The typical cross-section of the test section is shown in Fig. 6.

Three different bundles are fabricated for geometries A, B and C as shown in Fig. 7. The geometries are also specified in Table 3. Geometry A is mainly used to study the heat transfer and CHF of a single tube in a line of tubes. The heated tube or the unheateds tube can be drawn out of the test section from the back plate to produce different kind of spacing. Geometry B is a in-line tube bundle with pitch to diameter ratio of 1.5. Geometry C is a staggered tube bundle with 1.5 pitch to diameter ratio in both transversal and longitudinal directions. Theses two bundles are design to give the same solidity, which means the same number of tubes per unit cross section area of the bundle, in order to compare their heat transfer behavior at a same base.

As described in Table 3, the test bundle consists of an upstream unheated zone, a

heated zone, and an exit unheated zone. The tubes in the unheated zone are solid Aluminum tubes, while the tubes in the heated zone are 304 stainless steel seamless tubes. The inlet unheated zone is used to stabilize the flow stream and to allow a smoth flow transition from the inlet plenum to test bundles. It is also designed to compare the pressure drop with that in the heated zone.

The casing of the test bundle is made of rectangular Aluminum duct with 660.4 mm length. The cross section of flow duct is 61.6 mm by 85.725 mm. The duct is vertically orientated in the flow loop with Freon-113 flowing against gravity. Glass windows (3/4 inches thick pyrex No. 7740 glass) are installed in several locations to enable visual observation, lighting and photographic recording of flow pattern. The front window openings are installed with the 2.5 inches diameter pyrex glasses. The side window openings are installed with 1.75 inches diameter pyrex glasses. A 1.5 inch level shift between two sides windows is made to obtain a better lighting condition. The 1/16 inches thick neoprene rubber gaskets between the glasses and the Aluminum casing, and the Teflon tape are used to avoid the direct contact of pyrex glass and Aluminum casing and to seal the test section.

The changeable stainless stell back plate (3/4 inches thick) is attachecd to the Aluminum casing. The back plate is fitted with electrically heated tubes of 19.05 mm (3/4 inches) diameter, and 0.508 mm (0.020 inches) wall thickness. The detail of the non-instrumented heating tube is illustrated in Fig. 8. The electrically heated tubes are silver-soldered onto two copper ends. These copper pieces and the central copper rod (0.281 inches diameter) serve as the electrical current passage. The central copper rod is silver-soldered on the copper head at one end and screwed to the copper buss bar at the open end. The Teflon disk mounted at the end of the copper pieces is used as the electrical insulation.

Each test bundle contains an instrumented tube in the heated zone. The peripheral temperature on this tube is measured by two J-type ungrounded stainless steel sheathed thermocouples of 1.588 mm (1/16 inches) diameter. In the instrumented heating tube, the Micarta tube which guard the central copper rod has a slot (1/8 inches wide) cut through it to provide access for thermocouples and ceramic insulator. Fig. 9 shows the detail of the instrumented heating tube assembly. Pressure taps and thermocouples are also installed at several locations in the test chamber to provide the flow field information.

Both the inlet plenum and the exit plenum are made of stainless 304 pipe of 101.6 mm (4 inches) diameter, 50.8 mm (2 inches) length. The inlet plenum contains a perforated plate to homogenize the inlet vapor and liquid distribution of the test bundle. The exit plenum contains flow straightener to prevent the uneven flow distribution near the top of the bundle.

Power Supply

The D.C. electrical power for the test heating tubes is provided from a small welder and four large Westinghouse power supply in the Thermal Science Laboratory. The small welder supplies the finely controlled power up to 40 V, 300 Amp, while the large Westinghouse power supply gives up to 100 V and 1500 Amp.

The D.C. power from the Westinghouse welders is transported to the power pannel through two 2000 copper welder cables and then to the copper buss bar of the heating tube in the test bundle. A current shunt is installed in series with the test section such that the high current input to the test tube bundle can be accurately measured. For CHF experiment, two current shunts are used to measure the different heat fluxes supplied to the instrumented tube and surrounding tubes.

Instrumentation

All the measured temperatures in the test section are recored by the Accurex Autodata logger model Ten/5. The Autodata Ten/5 is a microprocessor-controlled data acquisition system which can scan 30 channels. It converts the output from thermocouples to precisely scaled DC voltage for measurement and displays the data in engineering units. A limited mathematics package that permits computation in real time. The alarms are also provided as a warning system in CHF studies. The data processing is programmed with a connected Zenith-19 cathode ray terminal. The photograph of the instrumentation rack is shown in Fig. 10.

The system temperatures in the loop are measured by J-type (1/16 inches) thermocouples and read directly from Autodata Ten/5 and digital temperature indicator (Omega Model 403A-C) through the selector switches. Two digital multimeters (Model HP-3465A) are also used in conjunction with two compensators (Omega Model MCJ-J) to obtain more accurate temperature measurements. Two moveable thermocouples as shown in Fig. 9 are used to measure the inside wall temperature of the heated tube. The junction of the J-type stainless steel sheathed unground thermocouples of 0.794 mm diameter are pressed against the inner wall by a plate-spring.

The power to the heating tubes is obtained by measuring the current through the heating tubes or the voltage drop across the precision shunt.

The flow rate through the test section is measured with a turbine flow meter (Model 80-0750, manufactured by Engineering Measurement Company Inc). A standard

preamplifier is supplied with the meter. The range of the output from the amplifier is 4 to 40 mAmp corresponding to 1.5 to 34 GPM. The current output from the meter is converted to mVolt (8 to 80 mv) and is fed to a Leeds & Northrop Model Speedomax H chart record. The line response of the meter can be described as :

$$Q\ (GPM) = 0.468\ V\ (mv) - 3.75$$

The system pressures are measured from 0.32 cm diameter taps located at several locations in the loop and in the test section. The pressure are recorded with two bourdon pressure gages 0 - 500 psi in 0.5 psi and 1.0 psi sub-divisions. The pressure drop through the tube bundles is also obtained by a calibrated pressure transducer (Model PB 415D-13) which is connected to a chart recorder (Sanborn Model 321).

REFERENCES

1. Yao, S. C. and Pfund, P. A., editor, FLUID FLOW AND HEAT TRANSFER OVER TUBE BUNdLES, ASME, 1979.

2. Schrock, V. E., editor, HEAT TRANSFER IN ROD BUNDLES, ASME, 1968.

3. Chen, K., "Longitudinal Laminar Flow in Asymmetrical Finite Bundles of Rods," Nuclear Engineering and Design, Vol. 25, 1973, pp. 207–216.

4. Mottaghian, R. and Wolf, L., "A Two Dimensional Analysis of Laminar Fluid Flow in Rod Bundles of Arbitrary Arrangement," Int. J. Heat Mass Transfer, Vol. 17, 1974, pp. 1121–1128.

5. Sparrow, E. M., loeffler, A. L. JR. and Hubbard, H. A., "Heat transfer to Longitudinal Laminar Flow Between Cylinder," J. Heat Transfer, 1961, pp. 415–422.

6. Wong, S. and Chen, K., "On the Two Dimensional Analysis of Fluid Flow and Heat Transfer in Rod Bundles with Arbitrary Arrangement," Nuclear Science and Engineering, Vol. 77, 1981, pp. 92–106.

7. Happel, J., "Viscous Flow Relative to Arrays of Cylinders," AIChE Journal, Vol. 5, 1959, pp. 174–177.

8. Whitaker, S., "Forced Convection Heat Transfer Correlations for Flow in Pipes, Past Flat Plate, Single Cylinders, Single Spheres, and for Flow in Packed Bed and Tube Bundles," AIChE Jouznal, Vol. 18, 1972, pp. 361–371.

9. Zukauskas, A., "Heat Transfer From Tubes in Crossflow," ADVANCED IN HEAT TRANSFER, Vol. 8, 1972, pp. 93–160.

10. Kays, W. and London, A. L., editor, COMPACT HEAT EXCHANGER, Macgraw Hill, 1964.

11. Gunter, A. Y. and Shaw, W. A., "A General Correlation of Friction Factors for Various Types of Surfaces in Crossflow," Trans. ASME, 1945, pp. 643–660.

12. Omohundro, G. A., Berglin, O.P. and Colburn, A. P., "Heat Transfer and Fluid Friction During Viscous Flow Across Banks of Tubes," Trans. ASME, 945, pp. 881–886.

13. Pierson, O. L., "Experimental Investigation of the Influence of Tube Arrangement on Convection Heat Transfer and Flow Resistance in Cross Flow of Gases over Tube Banks," Trans. ASME, 1937, pp. 563–572.

14. Huge, E. C., "Experimental Investigation of Effect of Equipment Size on Convection Heat Transfer and Flow Resistance in Cross Flow of Gases over Tube banks," Trans. ASME, 1937, pp. 574-581.

15. Berglin, O. P., Paris, E. S. and Hull, H. L., "A Study of Three Tube Arrangements in Unbaffled Tubular Heat Exchanger," Trans. ASME, 1949, pp. 369-374.

16. Ishihara, K. and Bell, K. J., "Friction Factor for In-Line Square Tube Banks at Low Reynolds Numbers," AIChE SYMPOSIUM SERIES, Vol. 68, 1972, pp. 74-80.

17. Lienhard, J. H. and Dhir, V. K., "Hydrodynamic Prediction of Peak Pool Boiling Heat Transfer From Finite Bodies," J. of Heat Transfer, Vol. 95, 1973, pp. 152-158.

18. Lienhard, J. H. and Eichhorn R., "Peak Boiling Heat Flux on Cylinders in A Cross Flow," Int. J. Heat Mass Transfer, Vol. 19, 1979, pp. 1135-9142.

19. Yilmaz, S., EFFECT OF VELOCITY ON BOILING FREON-113, PhD Dissertation, University of Illinois at Urbana-Champaign, 1979.

20. Yilmaz, S. and Westwater, J. W., "Effect of Velocity on Heat Transfer to Boiling Freon-113," J. of Heat Transfer, Vol. 102, 1980, pp. 26-31.

21. Polley, G. T., Ralston, T. and Grand J. D. R., "Forced Crossflow Boiling in An In-Line Tube Bundle," ASME paper No. 80-HT-46, 1980.

22. Cornwell, K. and Leong, L. S., "Heat Transfer Coefficient in A Reboiler Tube bundle," The Chemical Engineering, 1979, pp. 219-221.

23. Cornwell, K., Duffin, N. W. and Schuller, R. B., "An Experimental Study of The Fluid Flow on Boiling Within A Kettle Reboiler Tube Bundle," ASME paper No. 80-HT-45, 1980.

24. Cornwell, K. and Schuller, R. B., "A Study of Boiling Outside A Tube Bundle Using High Speed Photography," Int. J. Heat Mass Transfer, Vol. 25, 1982, pp. 683-690.

25. Cornwell, K., Schuller, R. B. and Einarson, J. G., "The influence of Diameter on Nucleate Boiling Outside Tubes," Int. Heat Transfer Conference, Vol. 4, 1982, pp. 47-53.

26. Palen, J. W., Yarden, A. and Taborek, J., "Characteristics of Boiling Outside Large-Scale Horizontal Multitube Bundles," AIChE SYMPOSIUM SERIES, Vol. 68, No. 118, 1972, pp. 50-69.

27. Bitter, R. C., "Heat Transfer From A Horizontal Tube with Transfer Flux of Evaporating Saturated R-11," Int. Inst. of Refrigeration, Heat and Mass Transfer in Refrigeration System and in Air Conditioning, 1972, pp. 97-107.

28. Wallner, R., "Boiling Heat Transfer in Flooded Shell-and-Tube Evaporators," Int. Inst. of Refrigezation, Heat and Mass Transfer in Refrigeration System and in Air Conditioning, 1972, pp. 185-191.

29. Hasan, M. M., Eichhorn, R. and Lienhard, J. H., " Burnout During Flow Across A Small Cylinder Influenced by Parallel Cylinder," Int. Heat Transfer Conference, Vol. 4, 1982, pp. 285-290.

List of Tables

List of Figures

Table 1 Specification of Freon-113 Loop

Item No.	Description
1	Main regulating valve
2	Test section
3	Ball valve
4	Condenser
5	Global control valve
6	Dégassing tank
7	Filter
8	Pump
9	Turbine flow meter
10	Preheater 1
11	Preheater 2
12	Preheater 3
13	Preheater 4
14	Freon-113 supply tank
15	Freon-113 accumulator

Table 2 Range of Experimental Conditions

Working fluid	Freon - 113
Heating tube	seamless 304 SS Tube
O.D. of heating tube	19.05 mm
Wall thickness of heating tube	0.508 mm
Test section	61.6 x 85.725 x 660.4 mm
Channel flow area	52.82 cm^2
Heat flux	0 - 537 KW/m^2
Inlet fluid quality	0 - 0.3
Superficial liquid velocity	0 - 0.34 m/sec
Volume flow rate	0 - 30 GPM
Mass flow rate	0 - 490 Kg/m^2
System pressure	0 - 40 psig

Table 3 Specification of Test Bundle

		Bundle Geometry		
		A	B	C
No. of row	Exit unheated zone	2	2	2
	Heated zone	8	8	8
	Upstream unheated zone	6	6	6
No. of column		1	3	3
Pitch to diameter ratio				
	X_T/D	1.5	1.5	1.5
	X_L/D	4.5	1.5	1.5
Heating length to diameter ratio (L/D)		2.6	2.6	2.6
D_H/D		$21/\pi$	$3/\pi$	$3/\pi$

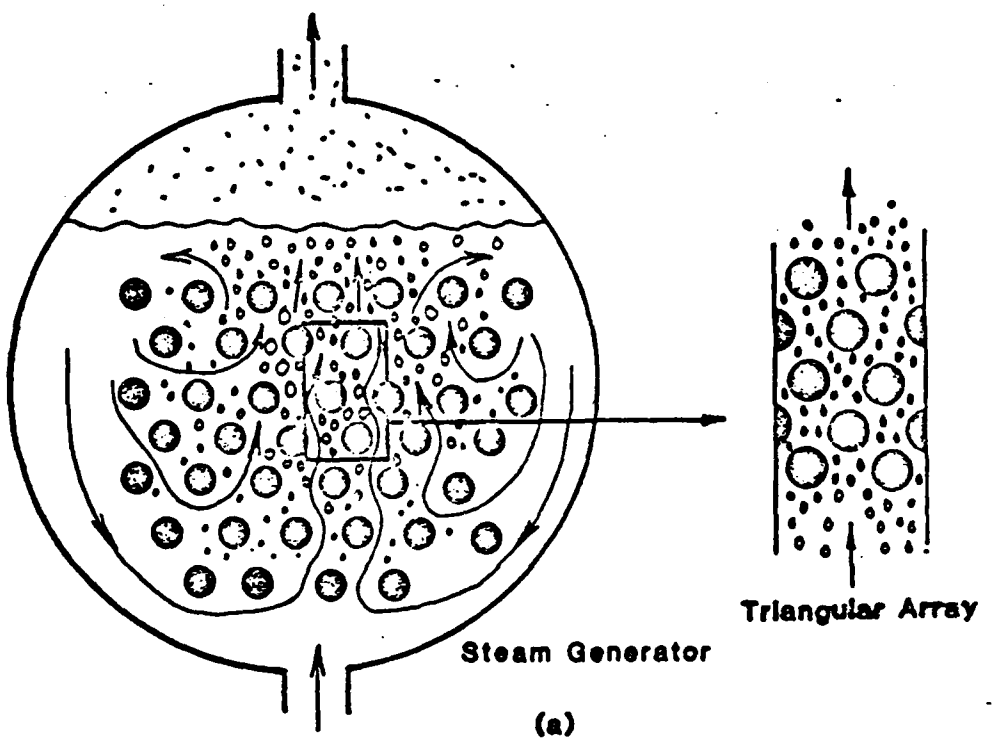
Triangular Array
Steam Generator
(a)

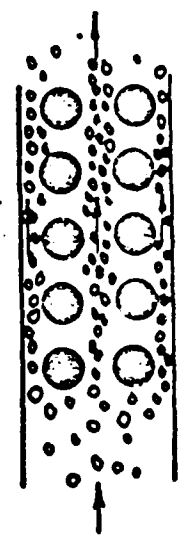
Vapor Streaming in Square Array
(b)

Fig. 1

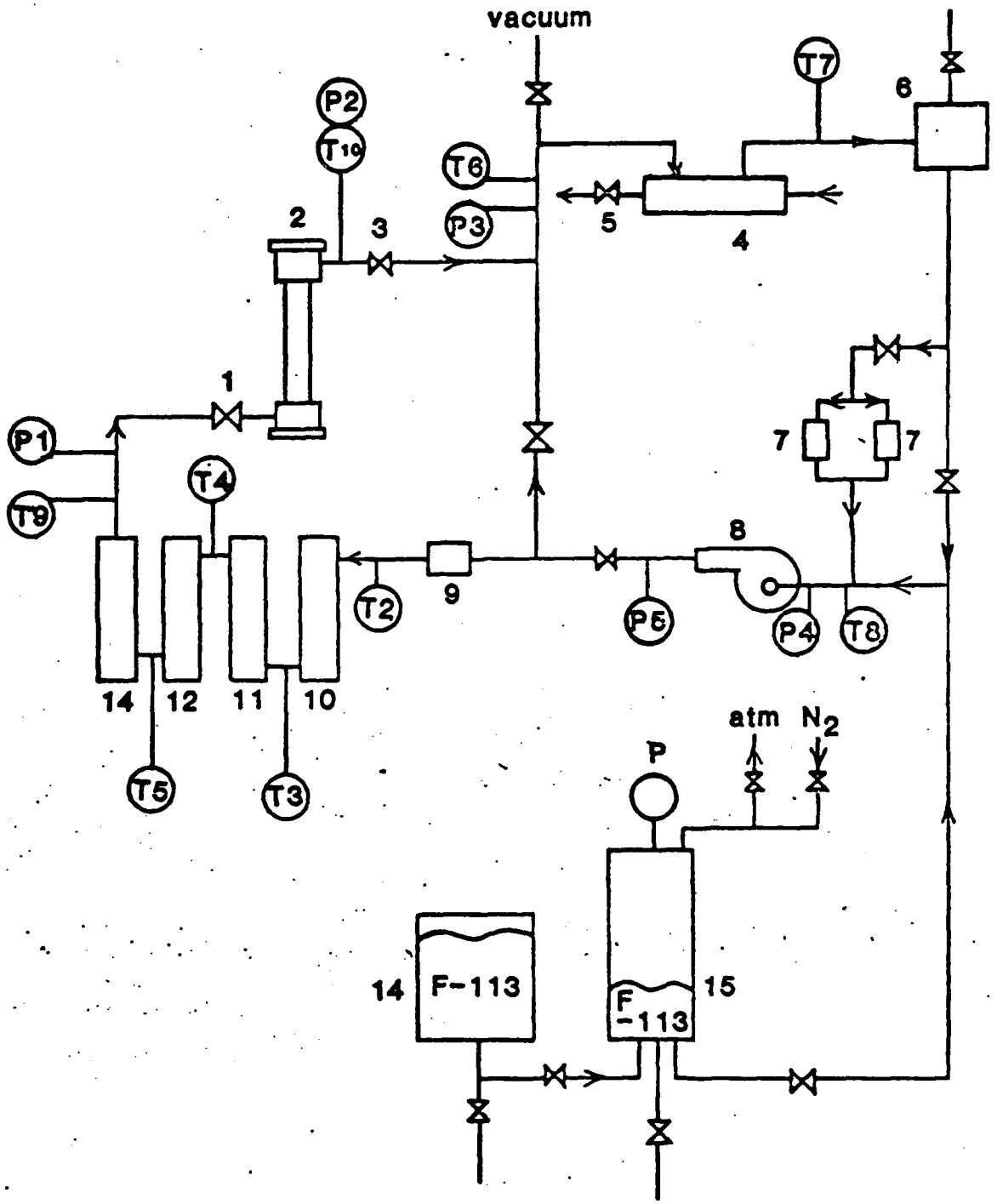

Fig 2: Schematic of Freon-1 .3 loop

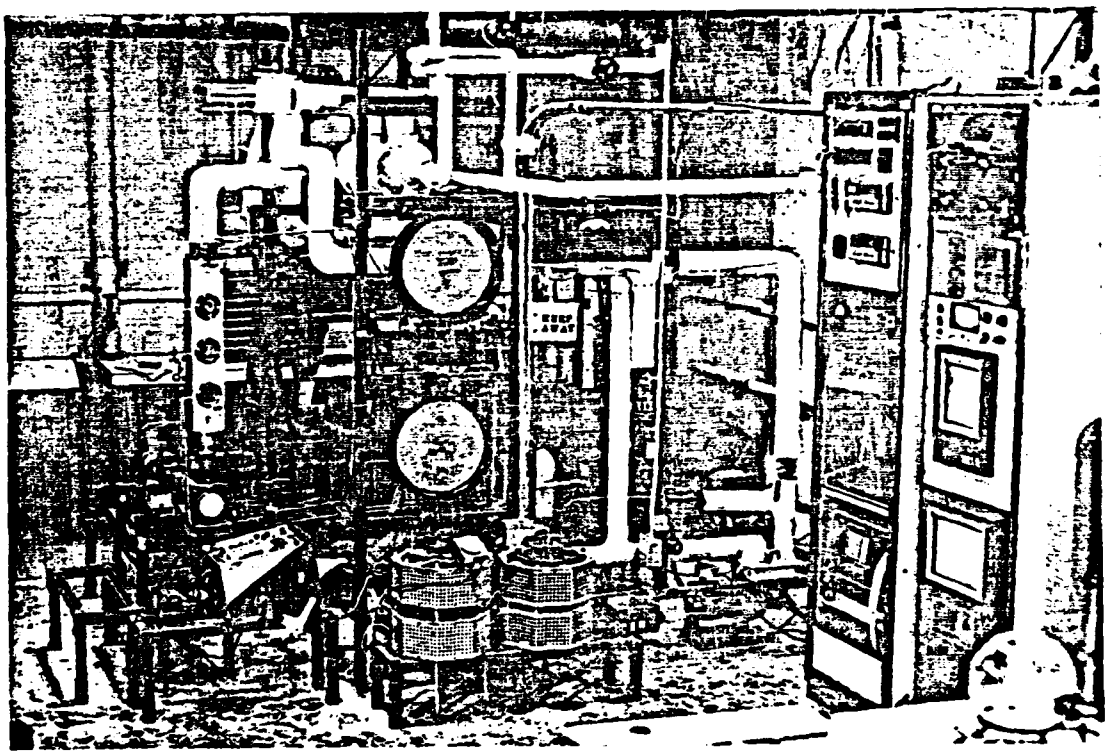

Fig. 3 Photograph of the Loop Assembly

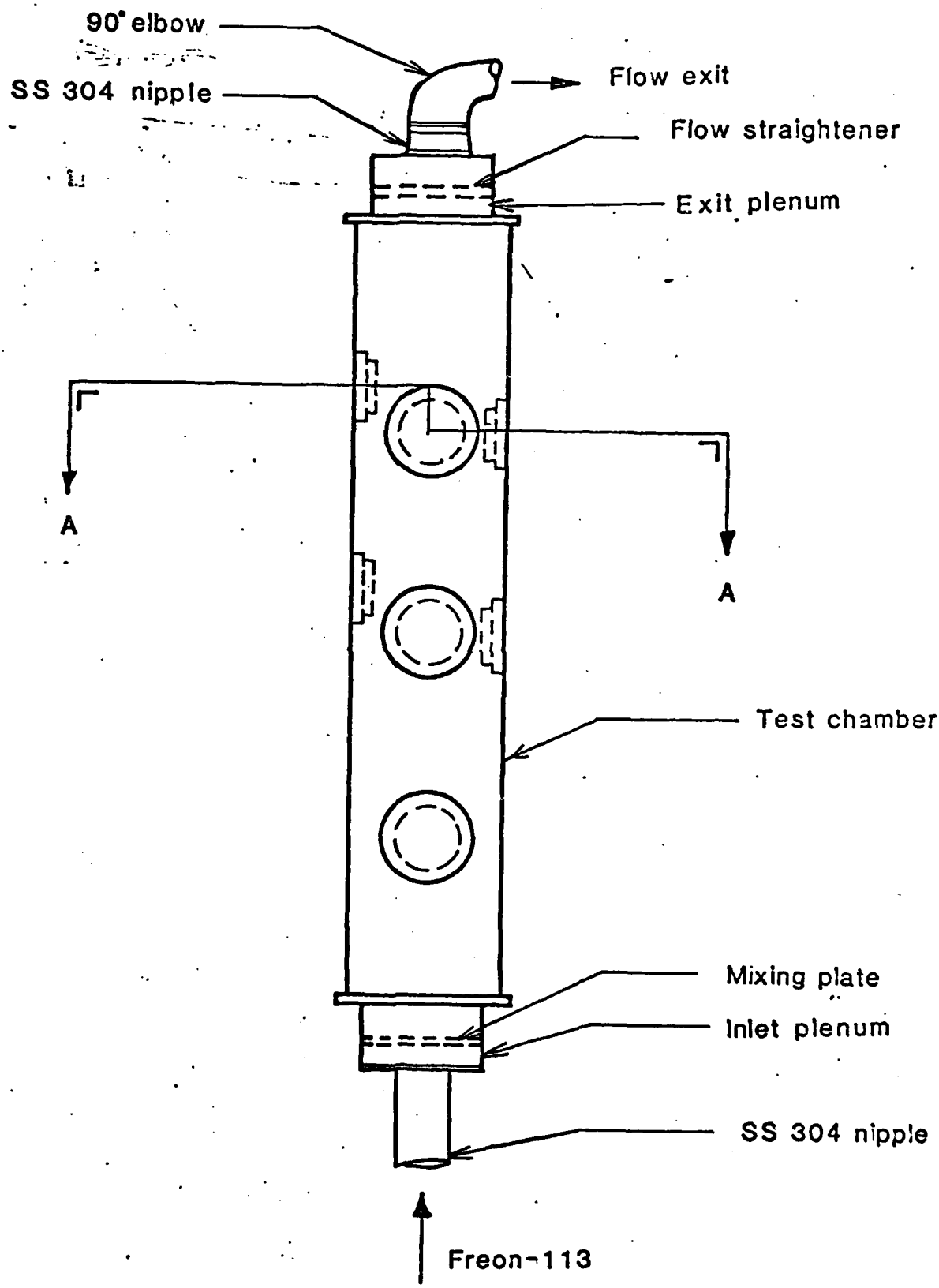

Fig. 4 Schematic of Test Section

AD-A136 721 CROSS FLOW BOILING IN TUBE BUNDLES(U) CARNEGIE-MELLON UNIV PITTSBURGH PA DEPT OF MECHANICAL ENGINEERING S C YAO OCT 83 N00014-79-C-0623 2/2

UNCLASSIFIED F/G 20/13 NL

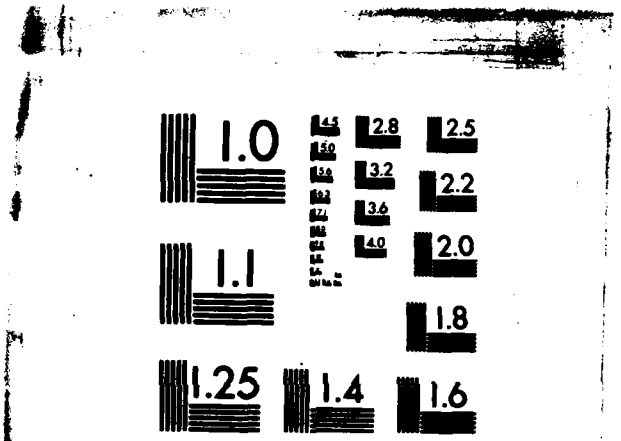

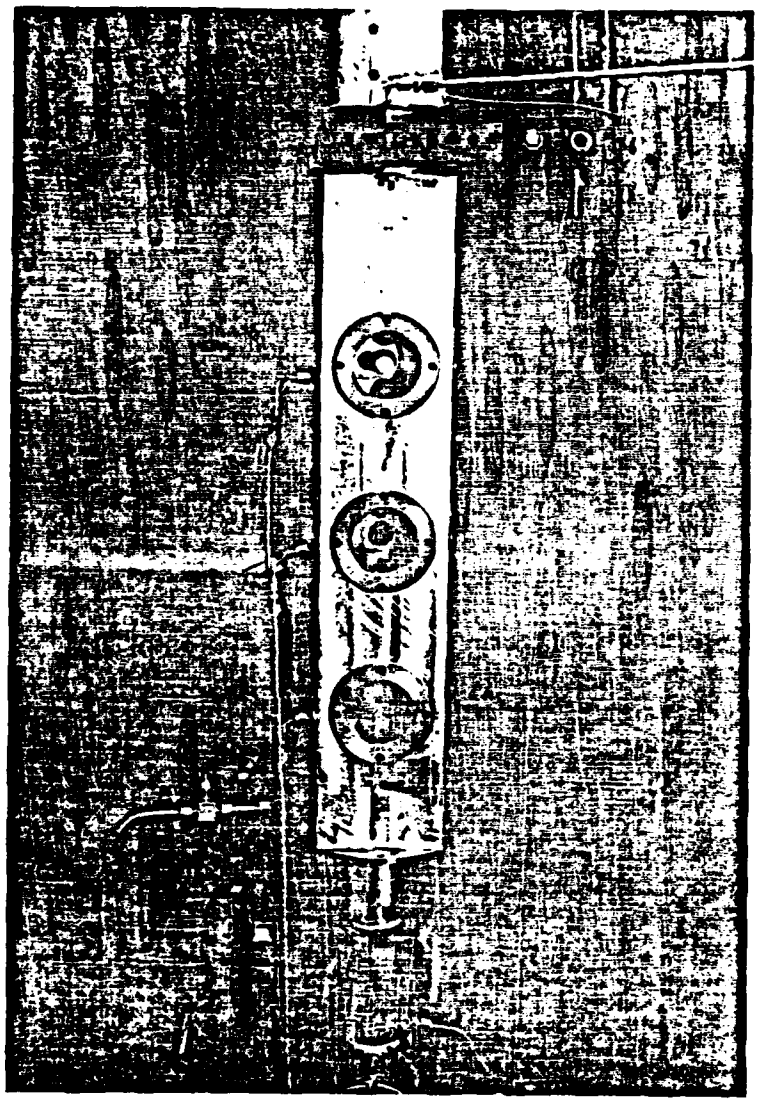

Fig. 5 Photograph of Test Section

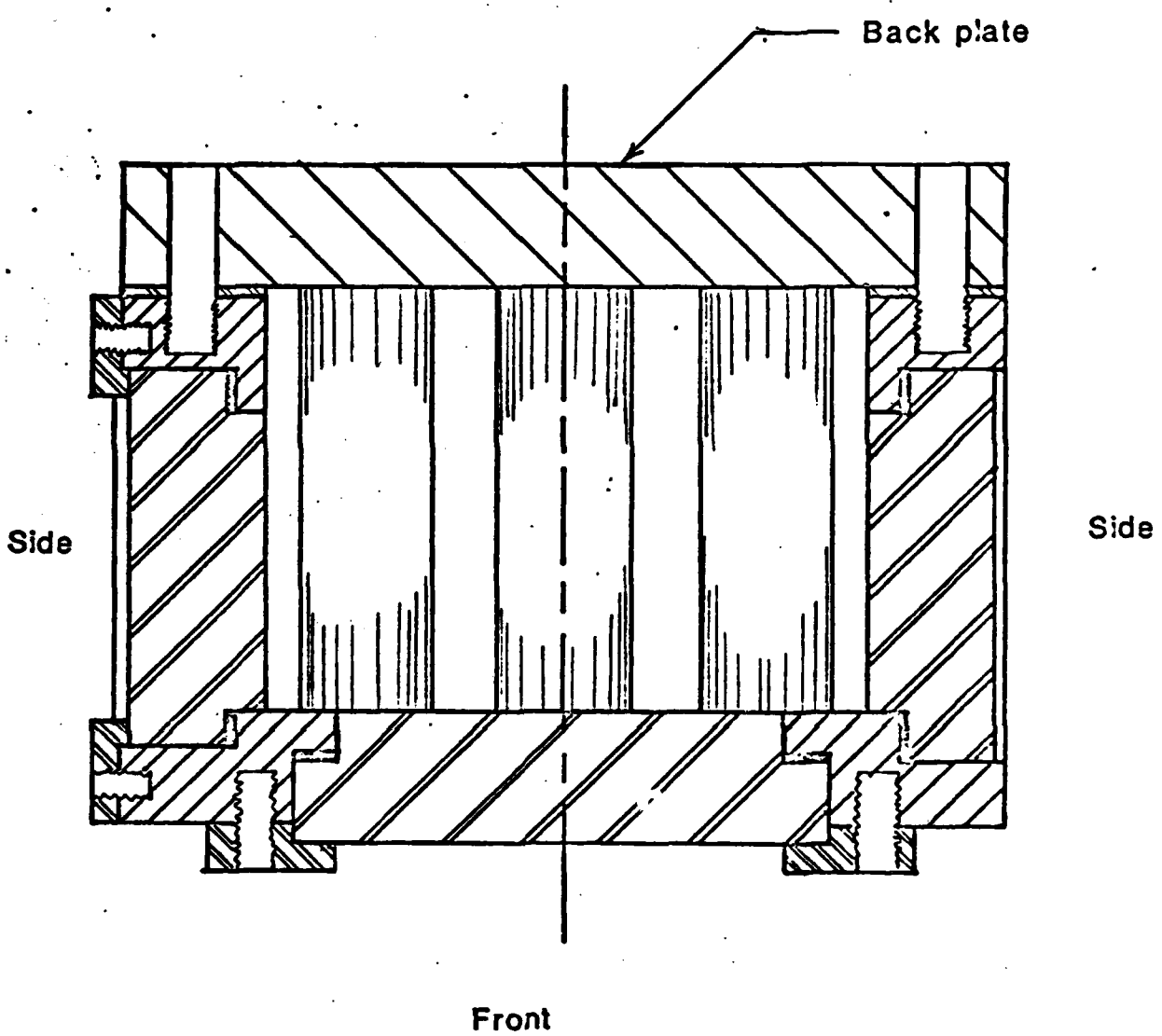

Fig. 6 Cross Section of Test Section

(view A-A)

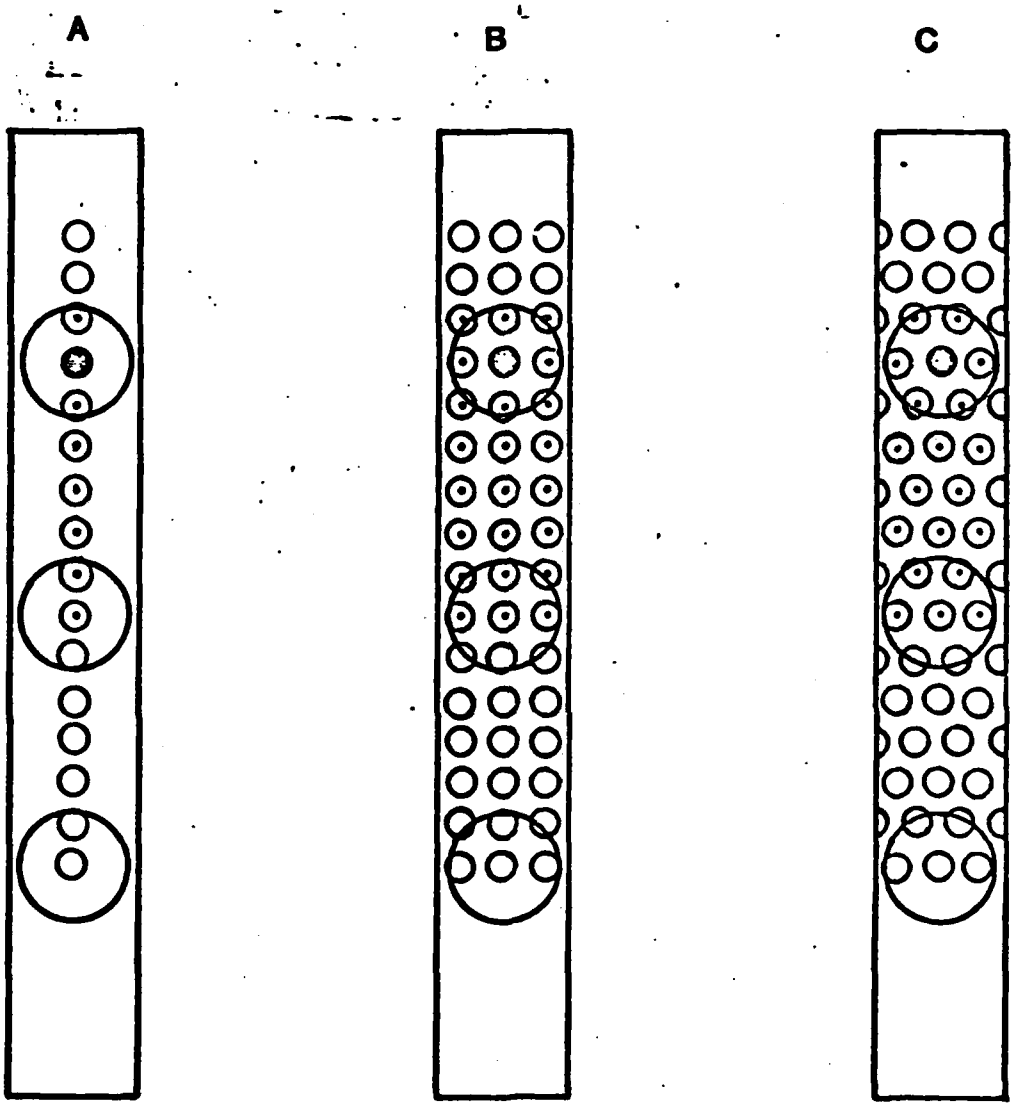

Fig. 7 Test Bundle Geometry

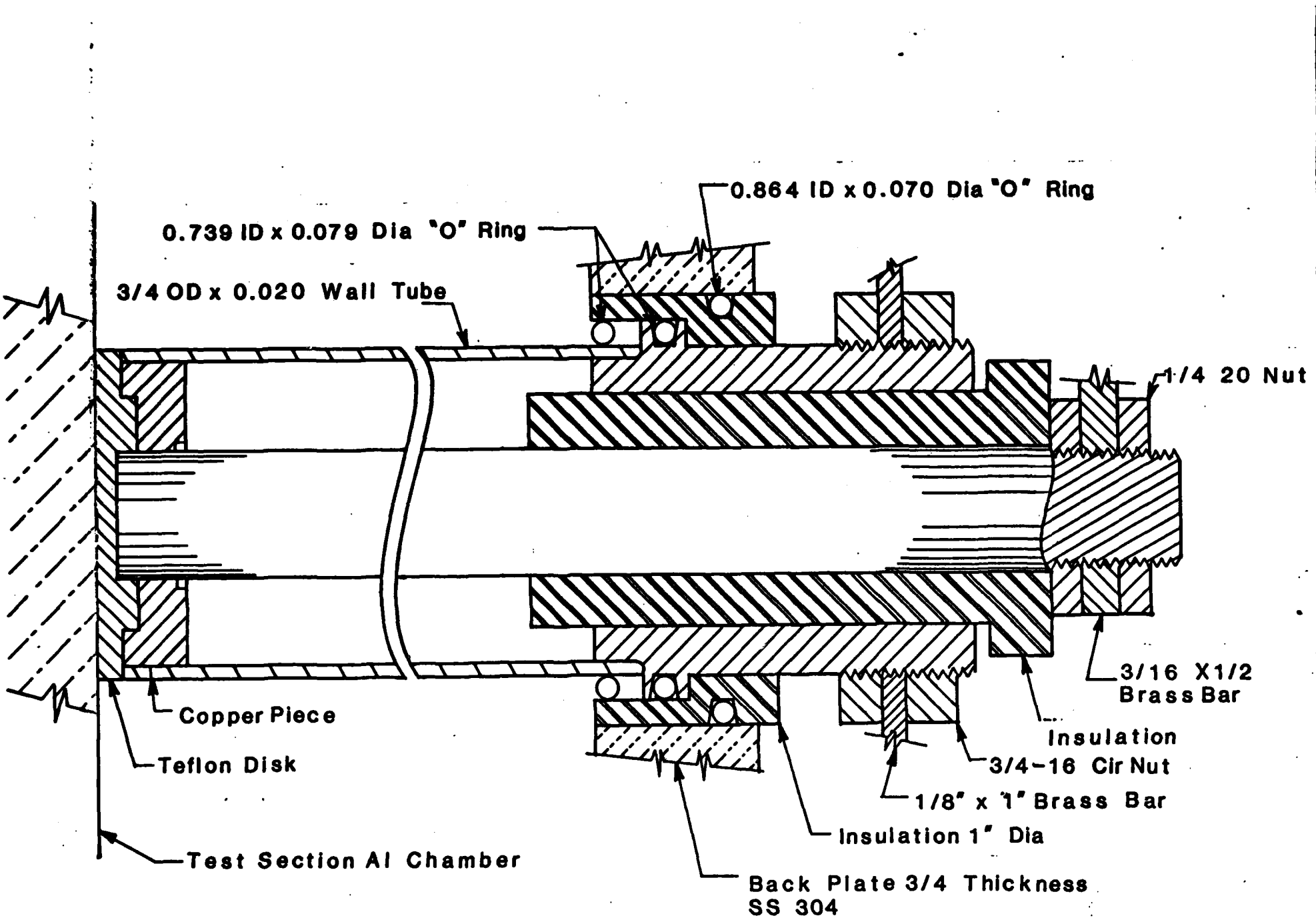

Fig. 8 Detail of Non-Instrumented Heating Tube

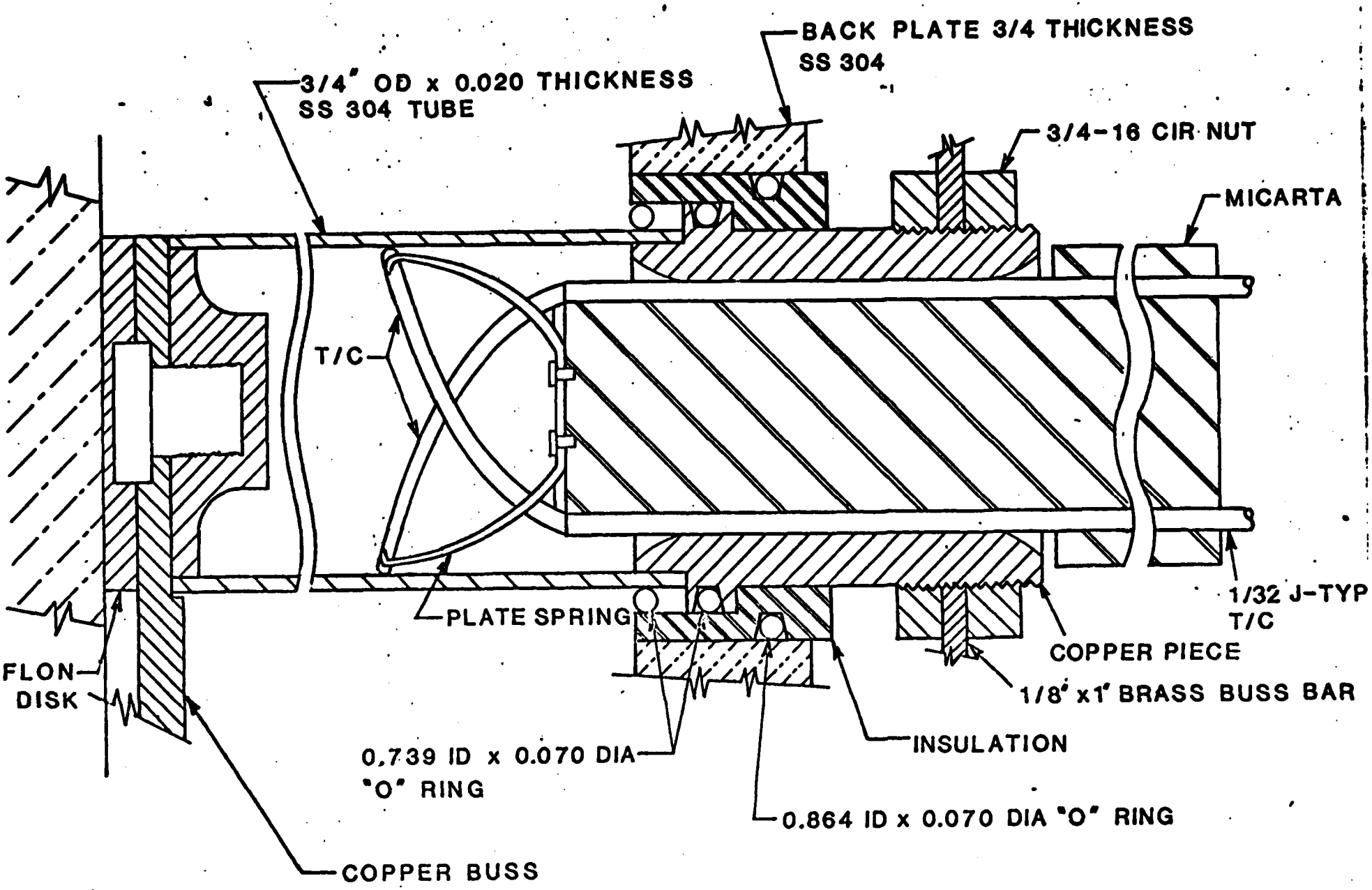

Fig. 9 Detail of Instrumented Heating Tube

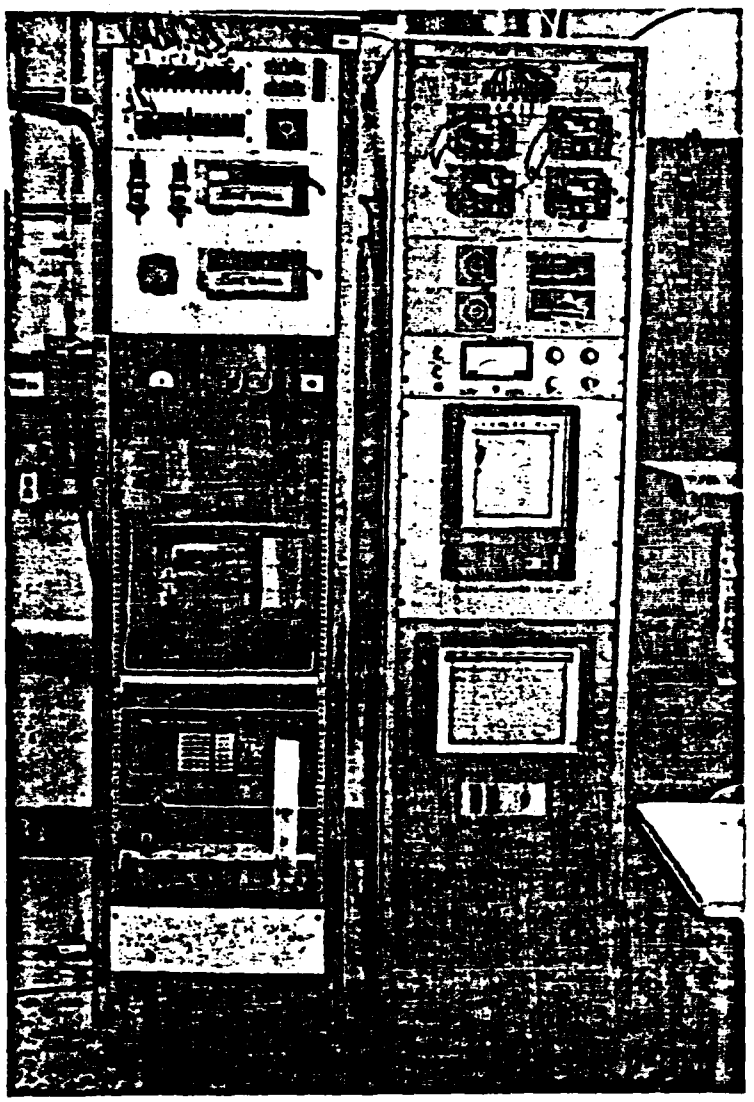

Fig. 18 Photograph of Instrumentation Racks

DISTRIBUTION LIST

HEAT TRANSFER

	One copy except as noted
Mr. M. Keith Ellingsworth Power Program Office of Naval Research 800 N. Quincy Street Arlington, VA 22217	5
Defense Documentation Center Building 5, Cameron Station Alexandria, VA 22314	12
Technical Information Division Naval Research Laboratory 4555 Overlook Avenue SW Washington, DC 20375	6
Professor Paul Marto Department of Mechanical Engineering US Naval Post Graduate School Monterey, CA 93940	
Professor Bruce Rankin Naval Systems Engineering US Naval Academy Annapolis, MD 21402	
Office of Naval Research Eastern/ Central Regional Office Bldg 114, Section D 666 Summer Street Boston, Massachusetts 02210	
Office of Naval Research Branch Office 536 South Clark Street Chicago, Ill. 60605	
Office of Naval Research Western Regional Office 1030 East Green Street Pasadena, CA 91106	
Mr. Charles Miller, Code 05R13 Crystal Plaza #6 Naval Sea Systems Command Washinton, DC 20362	

Steam Generators Branch, Code 5222
National Center #4
Naval Sea Systems Command
Washington, DC 20362

Heat Exchanger Branch, Code 5223
National Center #3
Naval Sea Systems Command
Washington, DC 20362

Mr. Ed Ruggiero, NAVSEA 08
National Center #2
Washington, DC 20362

Dr. Earl Quandt Jr., Code 272
David Taylor Ship R&D Center
Annapolis, MD 21402

Mr. Wayne Adamson, Code 2722
David Taylor Ship R&D Center
Annapolis, MD 21402

Dr. Win Aung
Heat Transfer Program
National Science Foundation
Washington, DC 20550

Mr. Michael Perlsweig
Department of Energy
Mail Station E-178
Washington, DC 20545

Dr. W.H. Theilbahr
Chief, Energy Conservation Branch
Dept. of Energy, Idaho Operations Office
550 Second Street
Idaho Falls, Idaho 83401

Professor Ephriam M. Sparrow
Department of Mechanical Engineering
University of Minnesota
Minneapolis, Minnesota 55455

Professor J.A.C. Humphrey
Department of Mechanical Engineering
University of California, Berkeley
Berkeley, California 94720

Professor Brian Launder
Thermodynamics and Fluid Mechanics Division
University of Manchester
Institute of Science & Technology
P088 Sackville Street
Manchester M601QD England

Professor Shi-Chune Yao
Department of Mechanical Engineering
Carnegie-Mellon University
Pittsburgh, PA 15213

Professor Charles B. Watkins
Chairman, Mechanical Engineering Department
Howard University
Washington, DC 20059

Professor Adrian Bejan
Department of Mechanical Engineering
University of Colorado
Boulder, Colorado 80309

Professor Donald M. McEligot
Department of Aerospace and Mechanical Engineering
Engineering Experiment Station
University of Arizona 85721

Professor Paul A. Libby
Department of Applied Mechanics and Engineering Sciences
University of California San Diego
Post Office Box 109
La Jolla, CA 92037

Professor C. Forbes Dewey Jr.
Fluid Mechanics Laboratory
Massachusetts Institute of Technology
Cambridge, Massachusetts 02139

Professor William G. Characklis
Dept. of Civil Engineering and Engineering Mechanics
Montana State University
Bozeman, Montana 59717

Professor Ralph Webb
Department of Mechanical Engineering
Pennsylvania State University
208 Mechanical Engineering Bldg.
University Park, PA 16802

Professor Warren Rohsenow
Mechanical Engineering Department
Massachusetts Institute of Technology
77 Massachusetts Avenue
Cambridge, Massachusetts 02139

Professor A. Louis London
Mechanical Engineering Department
Bldg. 500, Room 501B
Stanford University
Stanford, CA 94305

Professor James G. Knudsen
Associate Dean, School of Engineering
Oregon State University
219 Covell Hall
Corvallis, Oregon 97331

Professor Arthur E. Bergles
Mechanical Engineering Department
Iowa State University
Ames, Iowa 50011

Professor Kenneth J. Bell
School of Chemical Engineering
Oklahoma State University
Stillwater, Oklahoma 74074

Dr. James Lorenz
Component Technology Division
Argonne National Laboratory
9700 South Cass Avenue
Argonne, Illinois 60439

Dr. David M. Eissenberg
Oak Ridge National Laboratory
P.O. Box Y, Bldg. 9204-1, MS-0
Oak Ridge, Tennessee 37830

Dr. Jerry Taborek
Technical Director
Heat Transfer Research Institute
1000 South Fremont Avenue
Alhambra, CA 91802

Dr. Simion Kuo
Chief, Energy Systems
Energy Research Laboratory
United Technology Research Center
East Hartford, Connecticut 06108

Mr. Jack Yampolsky
General Atomic Company
P.O. Box 81608
San Diego, CA 92138

Mr. Ted Carnavos
Noranda Metal Industries, Inc.
Prospect Drive
Newtown, Connecticut 06470

Dr. Ramesh K. Shah
Harrison Radiator Division
General Motors Corporation
Lockport, New York 14094

Dr. Ravi K. Sakhuja
Manager, Advanced Programs
Thermo Electron Corporatio
101 First Avenue
Waltham, Massachusetts 02154

Mr. Robert W. Perkins
Turbotec Products, Inc.
533 Downey Drive
New Britain, Connecticut 06051

Dr. Keith E. Starner
York Division, Borg-Warner Corp.
P.O. Box 1592
York, PA 17405

Mr. Peter Wishart
C-E Power Systems
Combustion Engineering, Inc.
Windsor, Connecticut 06095

Mr. Henry W. Braum
Manager, Condenser Engineering Department
Delaval
Front Street
Florence, New Jersey 08518

Dr. Thomas Rabas
Steam Turbine-Generator Technical Operations Division
Westinghouse Electric Corporation
Lester Branch
P.O. Box 9175 N2
Philadelphia, PA 19113

Professor Daryl Metzger
Chairman, Mechanical and Energy
Systems Engineering
Arizona State University
Tempe, Arizona 85281

END

FILMED

2-84

DTIC